

**Alma Mater Studiorum - Università degli Studi di Bologna**

---

**SCUOLA DI SCIENZE**

Dipartimento di Chimica Industriale "Toso Montanari"

Corso di Laurea Magistrale in

**Chimica Industriale**

Classe LM -71- Scienze e Tecnologie della Chimica Industriale

**Polymer-liquid crystal interface: a molecular dynamics study**

Tesi di laurea sperimentale

**CANDIDATO:**

Federico Bazzanini

**RELATORE:**

**Chiar.mo Prof.** Claudio Zannoni

**CORRELATORI:**

Dr. Luca Muccioli

Dr. Mattia Felice Palermo

Sessione I

---

Anno Accademico 2012–2013

---





# Contents

<b>1</b>	<b>Introduction</b>	<b>3</b>
<b>2</b>	<b>Liquid Crystals</b>	<b>7</b>
2.1	Liquid crystals: an overview . . . . .	7
2.2	General properties of liquid crystals . . . . .	8
2.2.1	Nematic phase . . . . .	10
2.2.2	Cholesteric phase . . . . .	11
2.2.3	Smectic phase . . . . .	13
2.2.4	Columnar phase . . . . .	14
2.3	Liquid crystals applications . . . . .	16
<b>3</b>	<b>Molecular dynamics simulations</b>	<b>21</b>
3.1	Computer simulations . . . . .	21
3.2	Molecular Dynamics . . . . .	22
3.3	Hamiltonian dynamics . . . . .	23
3.4	Integrating the Equations of Motion . . . . .	25
3.4.1	The Verlet integrator . . . . .	26
3.5	Constant temperature molecular dynamics . . . . .	27
3.6	Constant pressure molecular dynamics . . . . .	29
3.7	Finite size effects and boundary conditions . . . . .	31
<b>4</b>	<b>Force fields for molecular simulations</b>	<b>33</b>
4.1	Molecular mechanics . . . . .	33
4.2	The Force Field . . . . .	33

4.3	Bonded interactions . . . . .	35
4.3.1	Torsion angles . . . . .	38
4.4	Nonbonded interactions . . . . .	39
4.4.1	Charges . . . . .	39
4.4.2	Lennard–Jones . . . . .	40
<b>5</b>	<b>Polymer-liquid crystals interfaces</b>	<b>43</b>
5.1	Polymer Film interfaces studies . . . . .	43
5.2	Liquid crystal Displays technology . . . . .	44
5.2.1	Twisted nematic displays . . . . .	44
5.3	Rubbing and LC alignment . . . . .	47
5.4	Clues on LCs alignment on polymers . . . . .	48
5.4.1	Polystyrene - liquid crystal studies . . . . .	50
5.4.2	Polymethyl-methacrylate - liquid crystal studies . . . . .	51
<b>6</b>	<b>Simulation study of the Polymer-LC interface</b>	<b>53</b>
6.1	Methods and simulation details . . . . .	54
6.2	Results and discussion . . . . .	55
6.2.1	Density profiles . . . . .	57
6.2.2	Characterization of polymer surfaces . . . . .	59
6.2.3	Molecular organization of 5CB . . . . .	63
6.2.4	Microscopic origin of 5CB surface alignment . . . . .	72
<b>7</b>	<b>Conclusions</b>	<b>77</b>
	<b>Bibliography</b>	<b>79</b>

# Chapter 1

## Introduction

Liquid crystals (LC) constitute an interesting class of soft condensed matter systems characterized by the counter-intuitive combination of fluidity and long-range order. LCs are known mainly for their applications in liquid crystal display (LCDs) however today, the interest in liquid crystals (LC) continues to grow pushed by their application in new technologies, for example in the field of medicine, optical imaging and biosensors<sup>[1]</sup>. An interesting unresolved question concerning LCs is the origin of their alignment on rubbed surfaces and in particular the polymer ones used in the display industry, that has remained a puzzle since its discovery in 1911<sup>[2]</sup>. Answering this question provides also the basis to optimize the operation of LCDs. Therefore, it is evident, that the alignment mechanism of LCs on polymer surfaces is not only an interesting scientific problem but also an important technological issue, since modern flat panel display performances depend on the ability of the manufacturer to prepare a substrate surface that will promote a particular type of alignment. Several techniques can be used to induce the LC to lie preferentially in a particular direction within the plane of the substrate surface. The traditional approach to create an aligning interface, is simply to rub the surface of a polymer layer that has been applied to coat a glass substrate. Although this rubbing technique has been used for decades, a rational optimization of this pro-

cess is still problematic, since the causes of alignment may be different. In general, the LC preferential orientation originates from symmetry breaking at the surface of substrate. Asymmetries in either the macroscopic topographical or in the microscopic molecular structure of the polymer surface have been proposed for its origin<sup>[3]</sup>. It is still a matter of study whether such alignment is primarily due either to the geometrical structure of the surface or to interaction between LC molecules and polymer chains, an effect that often makes the molecules line up along the rubbing direction<sup>[4]</sup>. In fact, on a macroscopic scale, rubbing a polymer surface can create grooves with a regular spacing of fractions of a micrometer. However, on a molecular scale, this process is also believed to order the polymer chains that lie in the surface by drawing them along the rubbing direction. Both grooves and chains stretching could, in principle, govern the alignment process. As a first approximation, also a almost flat crystalline surface of parallel chains can then be considered as having grooves on a scale of fractions of a nanometer along the chain direction. It is thus interesting to study if nanogrooves are effectively acting as LC molecules aligning agents. Today, thanks to the increase in computational resources, simulations have become an essential tool to understand and estimate the properties of liquid crystals, and of materials in general in the range of few nanometers. This work of thesis, is an attempt to find new evidences that might shed light on the origin of LC alignment on polymeric surfaces through molecular dynamics simulations (MD), allowing the investigation of the phenomenon at the atomic detail. Study can be framed as ideal prosecution of previous studies undertaken in the laboratory of Prof. Zannoni, where nematic and isotropic films of 5CB were analyzed at the interface with different flat, or slightly rough inorganic surfaces like silicon and silica both crystalline and glassy<sup>[5,6]</sup>. The relative importance of the arrangement of the polymeric chains in LC alignment was studied by performing MD simulations of a thin film of a typical nematic LC: 4-cyano-4'-pentylbiphenyl, 5CB, molecules in contact with two different, but very common, polymers such as Poly(methyl

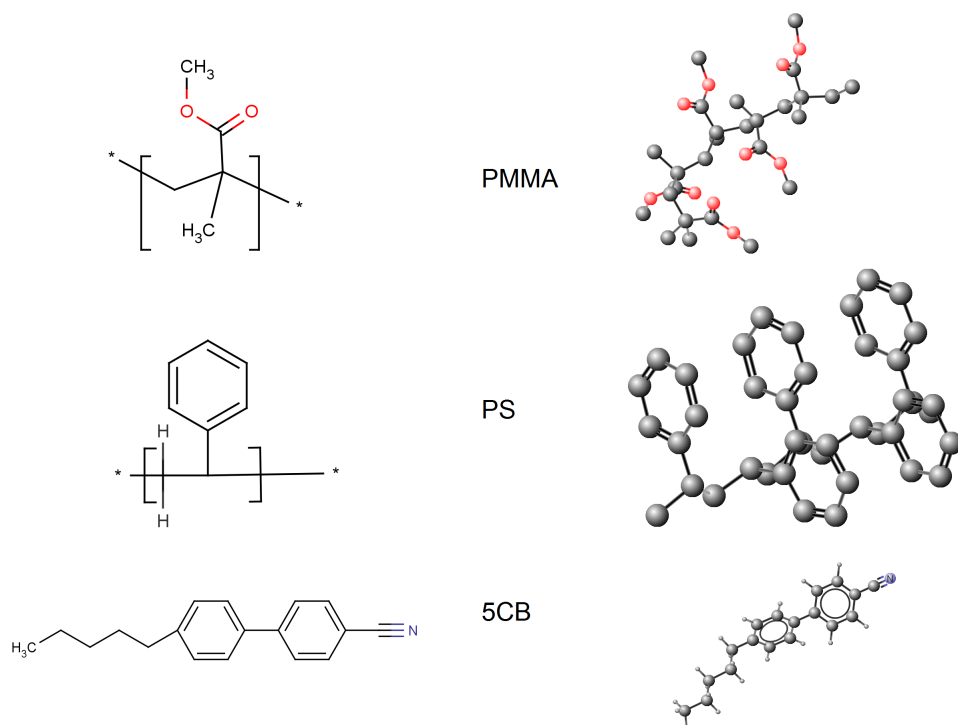


Figure 1.1: A schematic structure of the studied molecules.

methacrylate)(PMMA) and Polystyrene (PS), and with different degree of molecular order, (see Figure 1.1).



# Chapter 2

## Liquid Crystals

### 2.1 Liquid crystals: an overview

The study of liquid crystals (LC) began in 1888 when an Austrian botanist named Friedrich Reinitzer observed that a material known as cholesteryl benzoate had two distinct melting points. At a temperature of 145.5 °C, a solid crystal melted into a cloudy liquid until it reached 178.5 °C, where the cloudy liquid transformed into a transparent liquid. At temperatures higher than 178.5 °C, he noticed that the transparent liquid had properties of a common liquid. We know this temperature today as the clearing temperature  $T_c$  or the temperature at which the liquid crystal becomes an isotropic liquid. Later, a German physicist, Otto Lehmann, determined that the cloudy liquid observed had to be a new state of matter. It could not be labeled as just a liquid because ordinary liquids are isotropic; their properties are the same in all directions. The mesomorphic liquid crystal was first suggested by Lehmann (1889) to characterize this state of matter<sup>[7]</sup>. Such terms as mesomorphs or mesoforms, mesomorphic states, paracrystals, and anisotropic or ordered liquids or fluids have also been proposed and used in the literature. The history of the development of liquid crystals may be divided into different periods. The first period from their discovery in the latter part of the nineteenth century through to about 1925, the years

during which was overcome the initial diffuse skepticism about a state of matter in which the properties of anisotropy and fluidity were present at the same time. In this period the scientific production led to a classification of liquid crystals into different types. During the period from 1925 to about 1960, interest in liquid crystals was at a fairly low level. It was a niche area of academic research, and only relatively few, even if very active, scientists were devoted to extending knowledge of liquid crystals. Amongst other names of historical interest were, to name a few, Fréedericksz<sup>[8]</sup>, Zocher<sup>[9]</sup>, Ostwald, Lawrence<sup>[10]</sup>, Bernal and Sir W. H. Bragg<sup>[11]</sup>. Two world wars and their aftermaths contributed greatly to the retardation of the discovering in this new field of research. The period from 1960 until today is by contrast marked by a very rapid development in activity in the field, triggered of course by the first indications that technological applications could be found for liquid crystals.<sup>[12]</sup>

## 2.2 General properties of liquid crystals

Liquid crystals are a state of matter intermediate between that of a crystalline solid and an isotropic liquid. They possess many of the mechanical properties of a liquid, e.g., high fluidity, inability to support shear, formation and coalescence of droplets. At the same time, they are similar to crystals in that they exhibit anisotropy in their optical, electrical and magnetic properties. Liquid crystals which are obtained by melting a crystalline solid are called thermotropic. Liquid crystalline behavior is also found in certain colloidal solutions, such as aqueous solutions of tobacco mosaic virus, certain polymers and in water surfactant mixtures. This type of liquid crystal is called lyotropic. For the latter, concentration is the important controllable parameter, rather than temperature as in the thermotropic case.<sup>[13]</sup> Certain structural features are often found in molecules forming thermotropic liquid crystal phases, and they may be summarized as follows:

- the molecules have anisotropic shape (e.g. are elongated or disk-

like). Liquid crystallinity is more likely to occur if the molecules have flat segments, e.g. aromatic rings;

- a fairly rigid unsaturated backbone containing defines the alignment axis of the molecule;
- the existence of strong dipoles and easily polarizable groups in the molecule seems important;
- the groups attached to the extremities present different functions, for example, final flexible chains, provide fluidity to the compounds.

The multiple possible combinations of aromatic cores, aliphatic chains, and polar groups (see Figure 2.1) and the ingenuity of synthetic chemists has led to the discover of several types of LC phases (see<sup>[12]</sup>). In the following we describe briefly the most common ones.

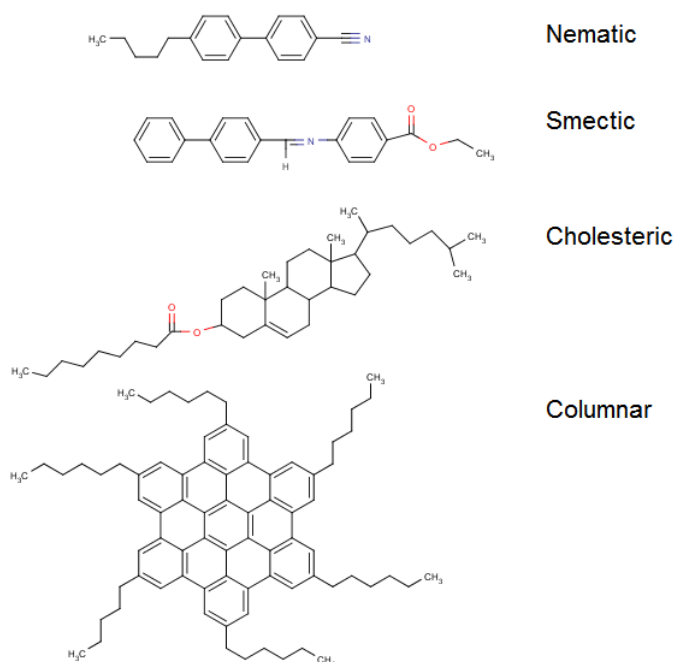


Figure 2.1: Structure of typical molecules that form liquid crystals.

### 2.2.1 Nematic phase

The nematic phase is characterized by long-range orientational order, i.e. the long axes of the molecules tend to align along a preferred direction, although, this direction may vary throughout the medium. Much of the interesting phenomenology of liquid crystals involves the dynamics of the preferred axis, which is defined by a vector  $\mathbf{n}(\mathbf{r})$  giving its local orientation. This vector is called a *director*. Since its magnitude has no significance, it is taken to be unity. There is no long-range order in the positions of the centers positional mass of the molecules of a nematic, but a certain amount of short-range order may exist as in ordinary liquids. Most nematics are uniaxial: when the director is aligned, e.g. with the help of an external field, an arbitrary rotation around the axis of alignment does not change the LC properties. As fore the constituent molecules (mesogens) they typically have one axis that is longer, with the other two being equivalent (can be approximated as cylinders or rods). A simplified picture of the relative arrangement of the molecules in the nematic phase is shown in Figure 6.6left. On optical examination of a non aligned nematic, domains with different orientation of the director coexist. Some very prominent structural perturbations appear as threads from which nematics take their name (Greek "*νημα*" means thread). These thread-like topological defects can be recognized when observing a nematic phase through a polarized light microscope, as shown in Figure 2.3. Conversely, in a typical computer atomistic simulation of LCs a monodomain is always obtained, due to the inevitably small sample size.

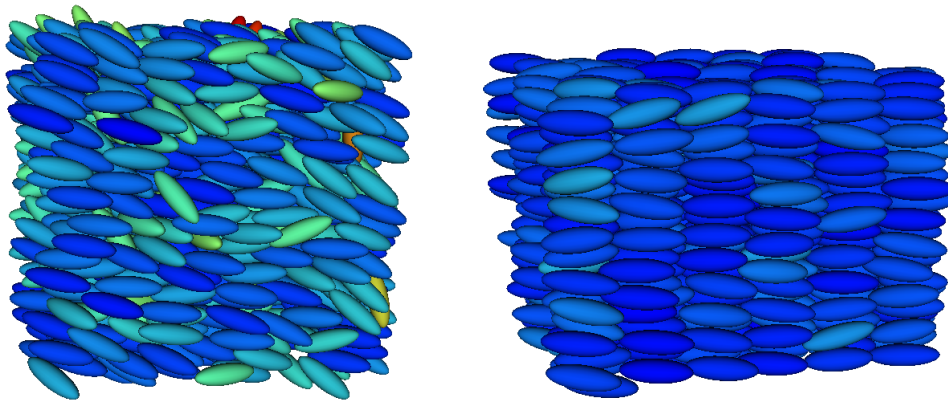


Figure 2.2: Alignment in a nematic phase (left) and smectic phase (right). The long molecules are, here, symbolized by ellipsoids.

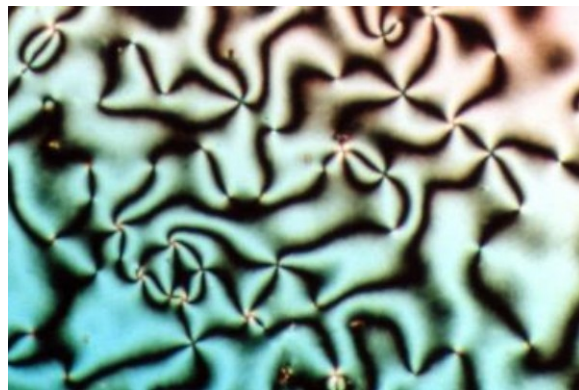


Figure 2.3: Typical schlieren textures of nematic liquid crystals observed through a polarized light microscope<sup>[14]</sup>.

### 2.2.2 Cholesteric phase

The cholesteric phase very similar to the nematic phase in having long-range orientation order and no long-range order in positions of the centers of mass of molecules. It differs from the nematic phase in that the director varies in orientation throughout the medium in a regular helical way. In any plane perpendicular to the twist axis the long axes of the molecules tend to align along a single preferred direction in this plane, but in a series of equidistant parallel planes, the preferred direction rotates of a fixed angle,

as illustrated in Figure 2.4. The secondary structure of the cholesteric is characterized by the distance measured along the twist axis over which the director rotates through a semi circle (since  $\mathbf{n}$  and  $-\mathbf{n}$  are indistinguishable). Cholesteric phase is formed by chiral liquid crystals or by doping them with optically active molecules, i.e. they have distinct right- and left-handed forms. The pitch of the common cholesterics is of the order of several hundreds nanometers, and thus comparable with the wavelength of visible light. The helical arrangement is responsible for the characteristic colors of cholesterics in reflection (through Bragg reflection of visible light by the periodic structure) and their very large rotatory power. The pitch can be quite sensitive to temperature, flow, chemical composition, and applied magnetic or electric field. Typical cholesteric textures are shown in Fig 2.5.

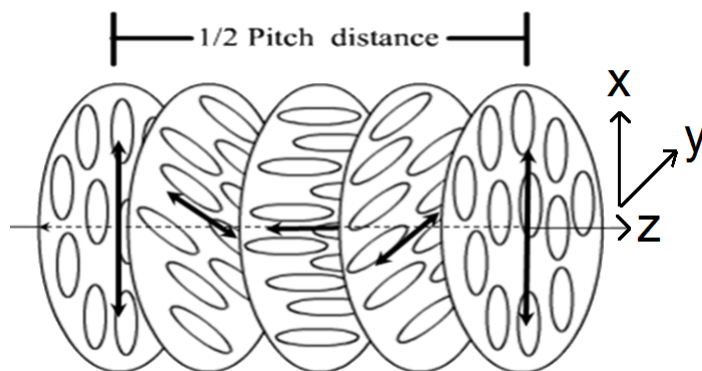


Figure 2.4: Schematic structure of chiral nematic (cholesteric) phase. Black arrows represent the director, which rotates perpendicularly to an axis in a helical manner. Molecules (represented as ellipsoids) can take any orientation, but are preferentially aligned to the director<sup>[15]</sup>.



Figure 2.5: Cholesteric fingerprint texture. The line pattern is due to the helical structure of the cholesteric phase, with the helical axis in the plane of the substrate<sup>[14]</sup>.

### 2.2.3 Smectic phase

Smectic phases have further degrees of order compared to the nematic one and are usually found at lower temperatures. The general rule appears to be that phases at lower temperature have a greater degree of crystalline order, for example, the nematic phase usually occurs at a higher temperature than the smectic phase; the term smectic comes from the greek word *σμηγμα* (smegma) which means soap, due to the preponderance of soap-like compounds that featured this peculiar phase at the time of their discovery. The important feature of the smectic phase, which distinguishes it from the nematic, is its stratification. The molecules are arranged in layers and exhibit some correlations in their positions in addition to the orientational ordering. A number of different classes of smectics have been recognized. In smectic A phase the molecules are aligned perpendicular to the layers, with no long-range crystalline order within a layer. The layers can slide freely over one another. Given the flexibility of layers, distortions are often present in smectic A phases, giving rise to optical patterns known as focal-conic textures, shown in Figure 2.8.

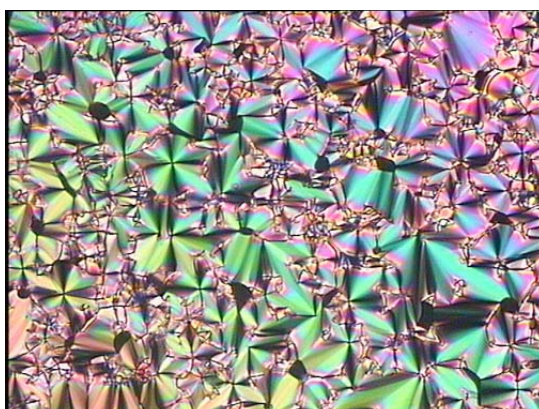


Figure 2.6: Typical focal-conic textures of smectic liquid crystals observed through a polarized light microscope. The micrograph show the fan shaped texture from the smectic A phase of a bent-shaped mesogens<sup>[14]</sup>.

In the smectic C phase the preferred axis is not perpendicular to the layers, so that the phase has biaxial symmetry. In smectic B phase there is long range hexagonal crystalline order within the layers, see Figure 2.7. The smectic phases typically occur in the order A, C, B as the temperature decreases.

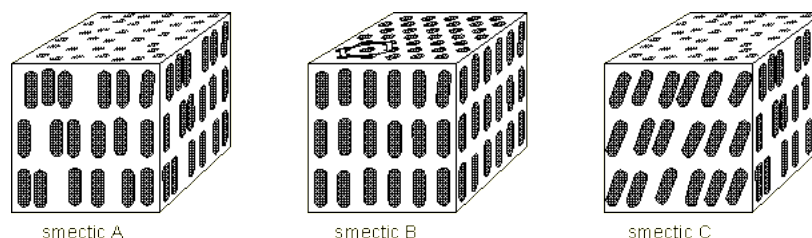


Figure 2.7: Schematic representations of different smectic liquid crystalline phase, respectively from left to right, smectic phases A, B and C.

## 2.2.4 Columnar phase

The columnar phase is a class of LC in which, flat than elongated molecules assemble into cylindrical structures. Originally, these kinds of liquid crystals were called discotic liquid crystals because the columnar structures was composed of flat-shaped discotic molecules stacked one-dimensionally.

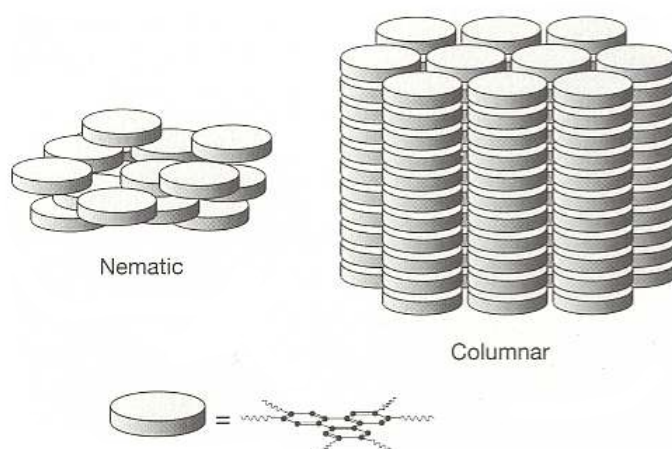


Figure 2.8: Schematic representation of a LC columnar phase.

Since recent findings provide a number of columnar liquid crystals consisting of non-discoid mesogens, it is more common now to classify this state of matter and compounds with these properties as columnar liquid crystals. Columnar liquid crystals are grouped by their structural order and the ways of packing of the columns. Nematic columnar liquid crystals have no long-range order and are less organized than other columnar liquid crystals. Other columnar phases are classified by their two-dimensional long-range order lattices since columns themselves may be organized into rectangular, hexagonal, tetragonal and oblique arrays. The first discotic liquid crystal was found in 1977 by the Indian group of Sivaramakrishna Chandrasekhar<sup>[16]</sup>. This molecule has one central benzene ring surrounded by six alkyl chains. Since then, a large number of discoid mesogenic compounds have been discovered in which triphenylene, porphyrin, phthalocyanine, coronene, and other aromatic cores are involved. In fact, the typical columnar liquid-crystalline molecules have a pi-electron-rich aromatic core attached by flexible alkyl chains. This structure is attracting particular attention for potential molecular electronics applications in which aromatic parts transport electrons or holes and alkyl chains act as insulating parts.

## **2.3 Liquid crystals applications**

Applications for LC are still being discovered and continue to provide effective solutions to many different problems. The most common application of liquid crystal technology is liquid crystal displays (LCDs). This field has grown into a multi-billion dollar industry, and many significant scientific and engineering discoveries have been made<sup>[17]</sup>. However there are several other, known, applications and in the following subsection some of the most important and promising ones are reported.

### **Liquid Crystal Thermometers**

Chiral nematic (cholesteric) liquid crystals selectively reflect light with a wavelength corresponding to the pitch. Because the pitch is dependent upon temperature, the color reflected is also dependent upon temperature. Liquid crystals make it possible to accurately gauge temperature just by looking at the color of the thermometer. By mixing different compounds, a device for practically any temperature range can be built. The "mood ring", a popular novelty in the mid 1970s, took advantage of the unique ability of the chiral nematic liquid crystal. More important and practical applications have been developed in such diverse areas as medicine and electronics. Special liquid crystal devices can be attached to the skin to show a "map" of temperatures. This is useful because often, infected regions such as tumors, have a different temperature than the surrounding tissue. Liquid crystal temperature sensors can also be used to find bad connections on a circuit board by detecting the characteristic higher temperature.

### **Optical Imaging**

An application of liquid crystals that is only now being explored is optical imaging and recording. In this technology, a liquid crystal cell is placed between two layers of photoconductor. Light is applied to the photocon-

ductor, which increases the material conductivity. This causes an electric field to develop in the liquid crystal corresponding to the intensity of the light. The electric pattern can be transmitted by an electrode, which enables the image to be recorded. This technology is still being developed and is one of the most promising areas of liquid crystal research.

## **Biosensors**

Because a reorientation of the director has such dramatic consequences on the optical properties of a liquid crystal, and because the director alignment at an interface is so sensitive to the chemical and physical environment at the interface, liquid crystals have great potential for use in sensors.<sup>[18]</sup>

## **LC lasing**

The selective reflection of the wavelength given by the helical pitch, typical of cholesteric LC, can be exploited to realize lasers. LCs are used as resonator cavity. In this type of laser, it is possible to tune the output wavelength. This is achieved by smoothly varying the helical pitch, that, in turn, shifts the optical path length in the lasing cavity. Changing in the helical pitch can be obtained for instance, applying static electric field, varying the temperature, or doping the LC with particular molecules or by mechanically squeezing.

## **LC in nano- and micro-technology**

Recently a new era is starting for LC research in soft matter nano-, bio- and microtechnology.<sup>[1]</sup> The ease of controlling LC alignment over large areas is very attractive in organic materials for semiconductor devices and energy conversion.<sup>[19]</sup> With today focus in material science on nanostructured materials, the ability of thermotropic LCs, as well as lyotropic, to

self-assemble into structures that exhibit specific nanoscale arrangements extending in an ordered fashion over a much longer range is extremely attractive. Several approaches have been devised to take advantage of the liquid crystalline order for generating new functional materials, either by making the liquid crystal-generated order permanent via polymerization, gelation or glass formation, or by preparing a liquid crystalline sample such that a regular array of defects forms, which can then be used e.g. for positioning nano- or microparticles over large areas.

## **LC and colloids**

Assembly of colloidal particles in nematic liquid crystals is governed by the symmetry of building blocks and type of defects in the liquid crystalline orientation. Particles in a nematic act as nucleation sites for topological defect structures that are homotopic to point defects. The tendency for a minimal deformation free energy and topological constraints limit possible defect configurations to extended and localized defect loops. Recently it was discovered the possibility of binding colloidal nanoparticles with a controlled network of disclination lines. Nematic braids formed by such disclinations stabilize multi-particle objects and entrap particles in a complex manner. Observed binding potentials are highly anisotropic, showing string-like behavior, and can be of an order of magnitude stronger compared to non-entangled colloids. Controlling the assembly based on entangled disclination lines one can build multi-particle structures with potentially useful features (shapes, periodic structure, chirality, etc.) for photonic and plasmonic applications<sup>[20]</sup>.

## **LC fibers and elastomers**

A very new development in liquid crystal research that holds considerable application potential is the production of textile fibers functionalized with liquid crystal in the core to realize “smart textiles”. For instance, with

a cholesteric core we can produce non-woven mats with iridescent color that can be tuned (or removed) e.g. by heating or cooling.<sup>[21]</sup> The combination of liquid crystals and polymers is at the core also of the field of liquid crystalline elastomers.<sup>[22]</sup> Liquid Crystal Elastomers are rubbery networks composed of long, crosslinked polymer chains that are also liquid crystalline (LC) - nematic, cholesteric or smectic. They typically elongate in the presence of nematic (orientational) order, and reversibly contract when the order is lost (typically by heating, but also by illumination or absorption of solvent). The molecular shape change is mirrored in the mechanical shape changes of the solid that the chains constitute. The changes, driven by the temperature change, can be very large, up to 500 %.

## **Other Liquid Crystal Applications**

Liquid crystals have a multitude of other uses. They are used for nondestructive mechanical testing of materials under stress. This technique is also used for the visualization of RF (radio frequency) waves in waveguides. They are used in medical applications where, for example, transient pressure transmitted by a walking foot on the ground is measured. Low molar mass liquid crystals have applications including erasable optical disks, full color "electronic slides" for computer-aided drawing, and light modulators for color electronic imaging. As new properties and types of liquid crystals are investigated and researched, these materials are sure to gain increasing importance in industrial and scientific applications.



# Chapter 3

## Molecular dynamics simulations

### 3.1 Computer simulations

Experiment plays an important role in science. Magnetic resonance (NMR) or X-ray diffraction, allow, for example, the determination of the structure and elucidation of the function of molecules. Yet, experiment is generally possible only in conjunction with models and theories to analyze and interpret the raw data. Computer simulations have altered the traditional interplay between experiment and theory. The essence of the simulation is the use of computers to model a physical system. Calculations implied by a mathematical model are carried out by the machine and the results are presented in terms of physical properties. Since computer simulations deal with models, they may be classified as a theoretical method. On the other hand, physical quantities can be “measured” on a computer, justifying the term “computer experiment”. The advantage of simulations is the ability to expand the horizon of the complexity that separates “solvable” from “unsolvable”. Basic physical theories such as quantum, classical and statistical mechanics, lead to equations that cannot be solved analytically (exactly), except for a few special cases. It is intuitively clear that less accurate approximations become inevitable with growing complexity. It is also much harder to include explicitly the electrons in the model, rather than representing the atoms as balls and the bonds as springs. The use of

the computer makes less drastic approximations feasible. Thus, bridging experiment and theory by means of computer simulations makes possible testing and improving our models using a more realistic representation of nature. It may also bring new insights into mechanisms and processes that are not directly accessible through experiment. On the more practical side, computer experiments can be used to discover and design new molecules. Testing properties of a molecule using computer modelling, in some cases, as in the docking of substrates to proteins,<sup>[23]</sup> is faster and less expensive than synthesizing and characterizing it in a real experiment. Drug design by computer is today commonly used in the pharmaceutical industry.<sup>[24]</sup>

## 3.2 Molecular Dynamics

Molecular dynamics (MD) is a computer simulation technique that allows one to predict the time evolution of a system of interacting particles (atoms, molecules, granules, etc.). The basic idea is simple. First, for a system of interest, one has to specify a set of initial conditions (initial positions, velocities of all particles in the system) and interaction potential for deriving the forces among all the particles. Second, the evolution of the system in time can be followed by solving a set of classical equations of motion for all particles in the system. Within the framework of classical mechanics, the equations that govern the motion of classical particles are the ones that correspond to the second law of classical mechanics formulated by Sir Isaac Newton. MD is a deterministic technique: given initial positions and velocities, the evolution of the system in time is, in principle, completely determined (in practice, accumulation of integration and computational errors would introduce some uncertainty into the MD output). Since the 1970s, MD simulations have been widely used to study the structure and dynamics of many molecules and macromolecules in different states and phases. There are two main families of MD methods, which can be distinguished according to the model (and the mathemat-

ical formalism) chosen to represent a physical system. In the classical mechanics approach, molecules are treated as classical objects, closely resembling the “ball and stick” model. Atoms correspond to soft balls and bonds correspond to elastic sticks. The dynamics of the system is defined by laws of classical mechanics. Instead, quantum or first-principles MD simulations, which started in the 1980s with the seminal work of Car and Parrinello<sup>[25]</sup>, take explicitly into account the quantum nature of the chemical bond. The electron density functional for the valence electrons that determine bonding in the system is computed using quantum equations, whereas the dynamics of ions (nuclei with their inner electrons) is followed classically. Quantum MD simulations represent an important improvement over classical approach but they require huge computational resources (a few hundred atoms at most can be studied currently). Today only classical MD is practical for simulations of biomolecular systems comprising up to one million of atoms (even if this is a small number compared to order of magnitude of the Avogadro’s number of real samples). Although, depending on system size and the use of high performance computing (HPC) it is possible to simulate processes that last more than one microsecond, molecular dynamics simulations can be used to examine numerous problems in chemistry, physics, medicine and biology.

### **3.3 Hamiltonian dynamics**

Hamiltonian mechanics was first formulated by William Rowan Hamilton in 1833, starting from Lagrangian mechanics, a previous reformulation of classical mechanics introduced by Joseph Louis Lagrange in 1788. It is a generalization of Newton’s equations for a point particle in a force field. The Hamiltonian formulation is easier to simulate numerically than other formulations such as the Euler-Lagrange. The Hamiltonian of a system, that represents its total energy (which is the sum of kinetic and potential energy, traditionally denoted  $T$  and  $V$ , respectively), can be defined start-

ing from the Lagrangians  $L$  defined as the kinetic energy of the system minus its potential energy in the following way.

$$L = T - V = E \quad (3.1)$$

$$H(\mathbf{q}, \dot{\mathbf{q}}, t) = \sum_{i=1}^n (\dot{q}_i p_i) - L(\mathbf{q}, \dot{\mathbf{q}}, t) \quad (3.2)$$

where  $q_i$  is a generalized coordinate,  $p_i$  is a generalized momentum, that for most of the studied systems correspond to position  $r_i$  and momentum  $\mathbf{p}_i = m_i \mathbf{v}_i$ , with  $m_i$  being the mass of the  $i$ -th particle moving at the velocity  $\mathbf{v}_i$ .

As  $p_i$  and  $q_i$  are conjugate variables, an Hamiltonian system has always and even number of dimensions  $2N$ , therefore  $N$  integrals are necessary to specify a trajectory, following Hamilton's equations:

$$\dot{q}_i = \frac{\partial H}{\partial p_i} \quad (3.3)$$

$$\dot{p}_i = -\frac{\partial H}{\partial q_i} \quad (3.4)$$

$$\dot{H} = -\frac{\partial L}{\partial t} \quad (3.5)$$

These equations have stationary points when

$$\dot{q}_i = \frac{\partial H}{\partial p_i} = 0 \quad (3.6)$$

$$\dot{p}_i = -\frac{\partial H}{\partial q_i} = 0 \quad (3.7)$$

(When the system reaches a critical point of the Hamiltonian function, a total equilibrium point is found. i.e.  $\nabla H = 0$ ). A Hamiltonian system in absence of time dependent external fields is *conservative*, as the energy does not change as the system evolves.

$$\begin{aligned}
\frac{dH}{dt} &= \sum_{i=1}^n \left( \frac{\partial H}{\partial q_i} \frac{\partial q_i}{\partial t} + \frac{\partial H}{\partial p_i} \frac{\partial p_i}{\partial t} \right) \\
&= \sum_{i=1}^n \left( \frac{\partial H}{\partial q_i} \frac{\partial H}{\partial p_i} - \frac{\partial H}{\partial p_i} \frac{\partial H}{\partial q_i} \right) \\
&= 0
\end{aligned} \tag{3.8}$$

It can also be demonstrated that the Hamiltonian flows preserve the volume, so trajectories obtained belongs to the microcanonical (NVE, with constant number of molecules, volume and energy) ensemble.

### 3.4 Integrating the Equations of Motion

It is obvious that a good MD program requires an efficient and accurate algorithm to integrate Newton's equations of motion. The aim of the numerical integration is to find an expression that defines positions  $\mathbf{r}_i(t + \Delta t)$  at time  $(t + \Delta t)$  in terms of the already known positions at time  $t$ .

A numerical method is required to solve the integration of the differential equations. This is typically done by discretizing the variable  $t$  in small timesteps  $dt$  using finite difference methods. These are explicit methods, based on a Taylor expansion of the positions and momenta at a time  $t + dt$  (Equation 3.9), that use the state of the system at a time  $t$  to predict the state at a time  $t + dt$ :

$$\begin{aligned}
\mathbf{r}(t + dt) &= \mathbf{r}(t) + \dot{\mathbf{r}}(t)dt + \frac{\ddot{\mathbf{r}}(t)}{2}dt^2 + \dots \\
&= \mathbf{r}(t) + \mathbf{v}(t)dt + \frac{\mathbf{f}(t)}{2m}dt^2 + \dots
\end{aligned} \tag{3.9}$$

Finite difference methods are subject to truncation errors and round-off errors. The former arise because the algorithm is based on a truncated

Taylor series expansion, while the latter is due to the actual implementation of the algorithm, e.g. the precision of computer arithmetic. Finite difference algorithms can be classified as predictor and predictor-corrector algorithms.<sup>[26]</sup> In predictor methods, molecular coordinates are updated from results that are either calculated in the current step or that are known from previous steps. The Verlet and leap-frog algorithms are examples of predictor algorithms. Predictor-corrector algorithms consist of three steps. First, we predict positions, velocities and accelerations from the results of previous time steps. Second, we compute new accelerations on the predicted positions. Third, we use these new accelerations to correct the predicted positions and their time derivatives. The Gear algorithm is an example.<sup>[27]</sup>

### 3.4.1 The Verlet integrator

Because of its simplicity and stability, the Verlet algorithm<sup>[28]</sup> is commonly used in MD. It is based on the addition of two Taylor expansions at time  $(t + dt)$  and  $(t - dt)$ :

$$\mathbf{r}(t + dt) = \mathbf{r}(t) + \dot{\mathbf{r}}(t)dt + \frac{\ddot{\mathbf{r}}(t)}{2m}dt^2 + \frac{\dddot{\mathbf{r}}(t)}{6m}dt^3 + O(dt^4) \quad (3.10)$$

$$\mathbf{r}(t - dt) = \mathbf{r}(t) - \dot{\mathbf{r}}(t)dt + \frac{\ddot{\mathbf{r}}(t)}{2m}dt^2 - \frac{\dddot{\mathbf{r}}(t)}{6m}dt^3 + O(dt^4) \quad (3.11)$$

Summing equation 3.10 and 3.11 we obtain:

$$\mathbf{r}(t + dt) = 2\mathbf{r}(t) - \mathbf{r}(t - dt) + \frac{\ddot{\mathbf{r}}(t)}{m}dt^2 + O(dt^4) \quad (3.12)$$

Verlet's algorithm presents the following benefits:

- Integrating does not require the velocities, which are however used for the calculation of the energy evaluated with the formula obtained subtracting Taylor's expansions 3.10 and 3.11.

$$\mathbf{v}(t) = [\mathbf{r}(t + dt) - \mathbf{r}(t - dt)]/(2dt) \quad (3.13)$$

however, the error associated to this expression is of order of  $dt^2$  rather than  $dt^4$

- Expressions are time-reversible.
- At each time step a single evaluation of forces is needed.

### 3.5 Constant temperature molecular dynamics

As seen before, Hamilton equations lead to a trajectory in the microcanonical (NVE) ensemble. The instantaneous translational temperature  $T$  can be calculated from the average of the kinetic energy:

$$\langle K \rangle = \frac{1}{2} \left\langle \sum_i^N m v_i^2 \right\rangle \quad (3.14)$$

and exploiting the equipartition principle

$$\frac{3}{2} k T N = \langle K \rangle \quad (3.15)$$

$$\begin{aligned} T &= \frac{2}{3kN} \langle K \rangle \\ &= \frac{1}{3k} \left\langle \sum_i^N m v_i^2 \right\rangle \end{aligned} \quad (3.16)$$

Only after we perform simulations and calculate the average of the kinetic energy, do we can determine the temperature at which the simulations are carried out. Constant-temperature molecular dynamics methods have been developed to resolve this frustrating situation. Consider a physical system enclosed in another larger one. Between these two systems, particles exchanges is not allowed, but energy transfer is possible. The external

system is very large in comparison with the internal one and it is called a heat reservoir or heat bath. The temperature of this external system is fixed at  $T$ . The temperature of our physical system, in a thermodynamical sense, is the temperature  $T$  of the external system<sup>[29]</sup>.

Since the temperature is related to the kinetic energy, in order to control the temperature, the velocities of the particles in the simulated system must be adjusted. One way to do this is to directly rescale the velocity of each particle, as shown in the following equation:

$$\left(\frac{v_{new}}{v_{old}}\right) = \left(\frac{T_{ext}}{T_{old}}\right)^{\frac{1}{2}} \quad (3.17)$$

where  $v_{new}$  is the rescaled velocity,  $v_{old}$  is the velocity before the rescaling,  $T_{ins}$  is the instantaneous system temperature, calculated from equation 3.16, and  $T_{ext}$  is the temperature of the thermal bath. This approach, called velocity rescaling, is used also to equilibrate systems during the first part of MD run, before the production run starts and data are collected. Using this strategy, it is easy to subtract (or add) energy from (or to) the system. However, direct velocity rescaling method is far away from the actual mechanism of energy dissipation.<sup>[30]</sup> A relatively gentle approach is the Berendsen method<sup>[31]</sup>, where the velocity of the particle is gradually scaled by multiplying it by a factor  $\lambda$  given by:

$$\lambda^2 = 1 + \frac{\Delta t}{\tau} \left( \frac{T}{T_{old}} - 1 \right) \quad (3.18)$$

where  $\Delta t$  is the time step and  $\tau$  is the time constant of the coupling. In this way, the velocities of the particles are adjusted such that the instantaneous kinetic temperature  $T_{old}$  approaches the desired temperature  $T$ . The strength of the coupling between the system and the thermal bath is controlled through the use of an appropriate coupling time constant  $\tau$ . If rapid temperature control is desired, a small  $\tau$  can be chosen. Consequently, the value of  $\lambda$  will be large and the change in the velocity will be drastic. On the other hand, if weak coupling is needed, a large value can be as-

signed to  $\tau$ . Although the ensemble sampled by the Berendsen method is approximately the canonical ensemble, it does not rigorously reproduce the canonical distribution, as the condition of constant temperature does not correspond to the condition of constant average kinetic energy, i.e. the fluctuations of the temperature and kinetic energy follow different laws. However, these methods lead to trajectories whose average values correspond to the ones of the canonical ensemble, even if their fluctuations do not<sup>[32,33]</sup>.

### 3.6 Constant pressure molecular dynamics

Most experiments are performed at constant pressure instead of constant volume. If one is interested in simulating the effect of, for example, the composition of the solvent on the properties of a system, the volume of an N,V,T simulation must be adjusted to ensure that the pressure remains constant. For such system, it is therefore much more convenient to run the simulation at constant pressure. In order to carry out a constant pressure MD simulation, volume is considered as a dynamic variable that changes during the simulation. The pressure tensor of the system  $\mathbf{\Pi}$  is measured as the sum of the kinetic energy contribution (ideal gas) plus the interparticle energy contribution (the so called virial tensor  $\mathbf{W}$ ). The pressure  $P$  is then calculated from the trace of the pressure tensor:

$$P = \frac{1}{3}Tr(\mathbf{\Pi}) \quad (3.19)$$

$$\mathbf{\Pi} = \frac{1}{V} \left[ \sum_i^N m_i (v_i \otimes v_i) + \mathbf{W} \right] \quad (3.20)$$

$$\mathbf{W} = \sum_{i=1}^N \mathbf{r}_i \otimes \mathbf{f}_i \quad (3.21)$$

If a cutoff scheme is used to perform simulations, the virial must be calculate from the pairwise forces<sup>[34]</sup>:

$$\mathbf{W} = \sum_{i=1}^N \sum_{j>i}^N \mathbf{r}_{ij} \otimes \mathbf{f}_{ij} \quad (3.22)$$

The barostat functioning scheme generally mimics the thermostats ones. The most common barostats are the “weak-coupling” barostat and the more complex Parrinello–Rahman ones<sup>[35]</sup>. In fact, the weak coupling scheme can be also applied to couple the system to a “pressure bath”<sup>[31]</sup>. The volume of the system is scaled to obtain a constant pressure close to that of the target pressure  $P_{ext}$  of the bath. The rate of change of pressure in a system is:

$$\frac{dP}{dt} = \frac{P_{ext} - P}{\tau_P} \quad (3.23)$$

$$P(t + \Delta t) = P(t) + [(P_{ext} - P(t))] \frac{\Delta t}{\tau_P} \quad (3.24)$$

where  $\tau_P$  is a coupling constant describing how strong the coupling between the bath and the system should be.  $P$  is the actual pressure at time  $t$ . To obtain the desired pressure change, the volume of the system is scaled with a factor  $\mu$ , defined as:

$$\mu = \left[ 1 + \frac{\Delta t}{\tau_P} \beta (P - P_{ext}) \right]^{\frac{1}{3}} \quad (3.25)$$

where  $\beta$  is the experimental isothermal compressibility of the system and  $\Delta t$  the time step. When the compressibility is not known, the water one’s is typically used, since  $\beta$  influences fluctuations frequency and not the

pressure itself, thus, most of the liquids have similar values. To run a simulation with a non-orthogonal box, the  $3 \times 3$  matrix  $\mathbf{h}$  has to be used, with its lines being the simulation axes and the determinant being the cell volume. The variation matrix  $\mathbf{M}$  is then obtained from the the pressure tensor:

$$\mathbf{M} = \left[ \frac{\beta}{\tau_P} (\mathbf{\Pi} - P_{ext} \mathbf{I}) \right] \quad (3.26)$$

The new (scaled)  $\mathbf{h}$  matrix is given by:

$$\mathbf{h}(t + \Delta t) = \mathbf{h}(t) + \mathbf{M} \mathbf{h}(t) \quad (3.27)$$

The scaling of the coordinates is then performed in this way:

$$\mathbf{r}_{scaled} = \mathbf{h}(t + \Delta t) \mathbf{h}^{-1}(t) \mathbf{r} \quad (3.28)$$

### 3.7 Finite size effects and boundary conditions

There are two different approaches to consider boundaries of the simulated system. One possibility is doing nothing special: the system simply terminates, and atoms near the boundary would have less neighbors than atoms inside. In other words, the sample would be surrounded by surfaces. Unless the aim is to simulate a cluster of atoms, this situation is not realistic. No matter how large the system is, its number of atoms  $N$  would be negligible compared with the number of atoms contained in a macroscopic sample, and the ratio between the number of surface atoms and the total number of atoms would be much larger than in reality, causing surface effects to be much more important than what they should. A solution to this problem is to use periodic boundary conditions (PBC). If one of the particles is passing through one of the borders of the box, it suddenly appears on the opposite side, as depicted in Fig.3.1. The system could be viewed as an infinite number of copies of the box placed side by side

extending into space. The copy of a specific particle in a neighbouring box, is called its *periodic image*. The underlying geometry does not need to be a cubic box. All shapes that fill the space when translated are valid. When computing the energy of the system only the energy in the central box is determined. The standard way of using a cut-off in periodic boundary conditions is to use the *minimum image convention* i.e., only particle interactions with the closest periodic image of all the other particles are counted. This gives a cut-off radius  $R_c$ , centered at the particle, of maximum  $1/2$  the box side length (In a cubic simulation box)<sup>[36]</sup>.

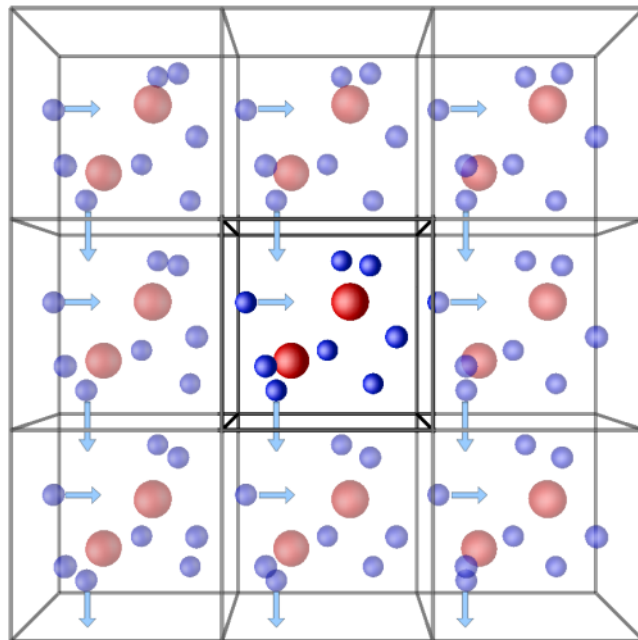


Figure 3.1: Schematic representation of the idea of periodic boundary conditions

# Chapter 4

## Force fields for molecular simulations

### 4.1 Molecular mechanics

The modelling of complex chemical system is still a hard challenge. Several sophisticated first-principles methods are available for simulating reactions and electronic processes to high accuracy but these are limited by their computational cost to small molecules. Since the majority of the problems to address in complex chemical systems involve many atoms, it is not feasible yet to treat these systems using quantum mechanic (QM) methods. A solution to reach high detail at low computational cost is Molecular Mechanics (MM), a technique which uses classical type models to predict the energy of a molecule as a function of its conformation. This allows, for instance, the prediction of equilibrium geometries and transition states and to evaluate relative conformers or different molecules energies.

### 4.2 The Force Field

The chemical information in the MM method is contained in the force field (FF). A FF is constituted by potential energy functions and a list of em-

empirical coefficients used to parameterise the intra- and inter- molecular energy for classes of molecules (e.g. alkanes, amino acids, etc.) Force fields parameters are often fitted against experimental data to reproduce a range of thermodynamic and structural properties for specific classes of molecules. In some cases, parameters may also be obtained via quantum mechanics calculations. The development of a FF is a very demanding task. This is an area of continuing research and many groups have been working over the past three decades to derive functional forms and to optimize parameters for potential energy functions of general applicability particularly to biological molecules. During the last few years, several force fields have been developed and optimized for protein simulations, such as OPLS/AMBER<sup>[37,38]</sup>, GROMOS<sup>[39]</sup> and CHARMM<sup>[40]</sup> force field, while the UFF<sup>[41]</sup> and MM3<sup>[42]</sup> force fields typically used to study small, isolated molecules (such as hydrocarbons). Most recent force fields that have obtained some success are the NERD<sup>[43]</sup> united atom FF and the more complex COMPASS force field<sup>[44]</sup>. FF developed to study chemical reactions, such as the REAXFF one<sup>[45]</sup> are also available. Recently, an enormous effort is being deployed in the development of the so called polarizable force fields, to include the electronic polarization for the treatment of nonbonded interactions in order to describe molecules in environments with significantly different polar character with high accuracy<sup>[46]</sup>. Molecular mechanics assumes the energy of a molecule to arise from a few, specific interactions as shown in Equations 4.2–4.6. These interactions include the stretching or compressing of bonds beyond their equilibrium lengths and angles, torsional effects of twisting about single bonds, the Van der Waals attractions or steric repulsions of atoms that come close together, and the electrostatic interactions between partial charges. To quantify the contribution of each, these interactions can be modeled by a potential function that gives the energy of the interaction as a function of atomic positions. The total steric energy of the system of molecule can be written as a sum of intramolecular and intermolecular energy interactions:

$$U_{\text{total}} = U_{\text{bonds}} + U_{\text{angle}} + U_{\text{dihed}} + U_{\text{LJ}} + U_{\text{charge}} \quad (4.1)$$

$$U_{\text{bonds}} = \sum_{\text{bonds}} K_r^{t_i t_j} (r_{ij} - r_{eq}^{t_i t_j})^2 \quad (4.2)$$

$$U_{\text{angles}} = \sum_{\text{angle}} K_{\theta}^{t_i t_j t_k} (\theta_{ijk} - \theta_{eq}^{t_i t_j t_k})^2 \quad (4.3)$$

$$U_{\text{dihed}} = \sum_{\text{dihed}} V_{\phi}^{t_i t_j t_k t_l} [1 + \cos(n^{t_i t_j t_k t_l} \phi_{ijkl} - \gamma^{t_i t_j t_k t_l})] \quad (4.4)$$

$$U_{\text{LJ}} = 4 \sum_{i < j} f_{LJ}^{1,4} \epsilon_{t_i t_j} \left[ \left( \frac{\sigma_{t_i t_j}}{r_{ij}} \right)^{12} - \left( \frac{\sigma_{t_i t_j}}{r_{ij}} \right)^6 \right] \quad (4.5)$$

$$\text{where } \epsilon_{t_i t_j} = (\epsilon_{t_i} \epsilon_{t_j})^{\frac{1}{2}}, \quad \sigma_{t_i t_j} = \frac{\sigma_{t_i} + \sigma_{t_j}}{2}$$

$$U_{\text{charge}} = \sum_{i < j} f_q^{1,4} \frac{q_i q_j}{r_{ij}} \quad (4.6)$$

The energy contributes reported above are common to the majority of the currently used force fields (CHARMM, AMBER, GROMOS, OPLS ). The variables contained in Equations 4.2–4.6 are angles  $\theta_{ijk}$ , distances  $r_{ij}$  and dihedral angles  $\phi_{ijkl}$ ; all the other terms are force field parameters.

The first ‘bonded’ sum is over bonds between atom pairs; the second sum is over bond angles i.e. by three atoms; the third sums is over four atoms defining a dihedral. In the ‘nonbonded’ interactions (electrostatics and Lennard Jones), the summation is over atom couples  $i$  and  $j$ , with  $i < j$  to ensure that each interaction is not calculated twice.

### 4.3 Bonded interactions

The stretching potential for a bond between atoms A and B,  $U_{\text{bond}}$ , represents the energy required to stretch or compress any bond between two atoms (see Figure 4.1) given by the Taylor expansion:

$$U_{\text{bond}} = \sum_{\text{bonds}} K_1(r_{ij} - r_{eq})^2 + K_2(r_{ij} - r_{eq})^3 + K_3(r_{ij} - r_{eq})^4 + \dots \quad (4.7)$$

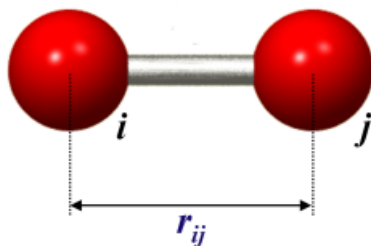


Figure 4.1: Graphical representation of bonded interactions.

Such expansions have incorrect limiting behavior at large distances, however, different FF methods retain different numbers of terms in this expansion, even though most of the times, only the first term is kept. In fact, a bond can be thought as a spring having its own equilibrium length,  $r_{eq}$ , and the energy required to stretch or compress it can be approximated by the potential for an ideal spring using the Hooke's law.

$$U_{\text{bond,Hooke}} = K(r_{ij} - r_{eq})^2 \quad (4.8)$$

where  $r_{ij}$  is the distance between the two bonded atoms and  $K$  is a force constant. The shape of the potential energy well will be parabolic (see Figure 4.2) and the motion will therefore tend to be harmonic.

A simple function with correct limiting behavior is the Morse potential, which is a convenient model for the potential energy of a diatomic molecule:

$$U_{\text{bond,Morse}} = D_e[1 - e^{-(r_{ij}-r_{eq})}]^2 \quad (4.9)$$

where  $D_e$  is the "equilibrium" dissociation energy of the molecule which is measured from the potential minimum of the potential energy and is equal to the experimentally dissociation energy. However, this potential

gives very small restoring forces for large  $r_{ij}$  values and therefore causes slow convergence in geometry optimization. It is a better approximation for the vibrational structure of the molecule than the quantum harmonic oscillator because it explicitly includes the effects of bond breaking, such as the existence of unbound states. This potential, unlike the preceding one, is asymmetric indicating that it is harder to compress a bond than to pull it apart.  $U_{angle}$  is the energy required to vary an angle between atoms  $i-j-k$ , defined as the angle between the bonds  $i-j$  and  $j-k$  from its equilibrium value. Once again, this system can be modeled as a spring, and the energy is given by the Hook's potential with respect to angle:

$$U_{angle} = K_{\theta}(\theta_{ijk} - \theta_{eq})^2 \quad (4.10)$$

Sometimes, another harmonic energy contribution,  $U_{bond-angle}$ , is calculated, that is the stretch-bend interaction energy that takes into account the observation that when a bond is bent, the two associated bond lengths increase.

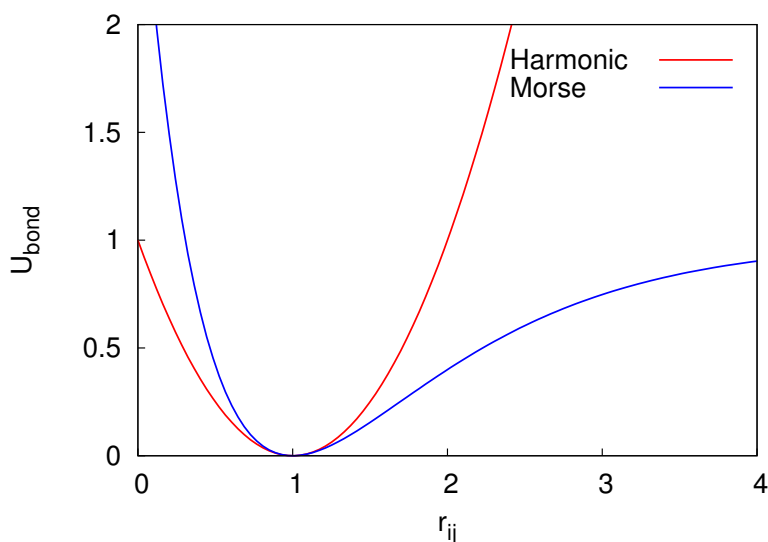


Figure 4.2: Morse and Hooke bond-potential as function of  $r_{eq} = 1$

### 4.3.1 Torsion angles

Torsion angles are distinguished in two types: proper torsion angles (dihedral) and improper torsion angles. If four atoms  $i$ - $j$ - $k$ - $l$  are given, the dihedral is defined as the angle between two planes containing respectively  $ijk$  and  $jkl$  (see Figure) 4.3.

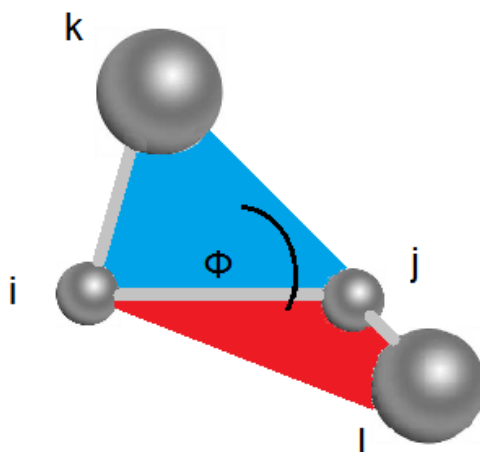


Figure 4.3: Dihedral angle,  $\phi$ , defined by four atoms  $i$ ,  $j$ ,  $k$  and  $l$ .

The dihedral angle between two planes is the angle between their two normal unit vectors  $n_{ijk}$  and  $n_{jkl}$  as can be seen by looking at the planes "edge on", i.e., along their line of intersection. Torsional energies  $U_{\text{dihed}}$  are usually important only for single bonds because double and triple bonds are too rigid to permit rotation. A traditional way to model the potential energy for a torsional rotation is the one introduced by Pitzer<sup>[47]</sup>:

$$U_{\text{dihed}} = V_n [1 + \cos(n \phi_{ijkl} - \gamma_n)] \quad (4.11)$$

where  $n$  is the number of maxima or minima in one full rotation,  $V_\phi$  is the half energy barrier to rotation (due to electronic repulsions or steric hindrance) and  $\gamma_n$  determines the angular offset. In the 1960's, when potential energy functions for proteins were first developed, it was found the Pitzer potential was insufficient to give a full representation of the energy

barriers of dihedral angle change. Today, most used torsional potential are expressed in the form of a sum of Pflizer terms with different  $n$ . Improper torsions, also called the out of plane terms, involve atoms that are not serially bonded but branched, like a the nitrogen atom in amines. The term depends on four atoms, but the atoms are numbered in a different order. Improper torsion is used to describe the energy of out-of-plane motions. It is often necessary for planar groups, such as  $sp^2$  hybridized carbons in carbonyl groups and in aromatic rings, because the normal torsion terms is not sufficient to maintain the planarity.

## 4.4 Nonbonded interactions

In addition to the bonded interactions between atoms described above, force fields also contain non-bonded interactions. Non-bonded interactions act between atoms in the same molecule and those in other molecules. Force fields usually divide non-bonded interactions into two: electrostatic and Van der Waals interactions. As the name suggests, non-bonded interactions act between atoms which are not linked by covalent bonds. The non-bonded terms are much more computationally expensive to calculate than bonded interaction. In fact, a typical atom is bonded to only a few of its neighbors, but interacts with every other atom in the molecule. Thus, the number of non bonded terms to calculate is not proportional to the number of atom ( $N_A$ ) but to  $N_A^2$ , and it is important to optimize the calculation of this type of interaction.

### 4.4.1 Charges

Electrostatic forces are essential in evaluating intermolecular interactions. In many respects, electrostatic interactions are one of the biggest problems for computational studies of soft matter, as they are long range and dependent on the properties of the surrounding medium. Usually, to take

these forces in account during the simulation, charges are placed on each atomic nucleus. Charges on adjacent atoms (one or two covalent bonds) are normally made invisible to one another, since the interactions between these atoms is already described with the stretching and bending terms. The electrostatic interactions are modeled with a Coulomb potential:

$$U_{\text{charge}} = \frac{1}{4\pi\epsilon_0\epsilon_r} \frac{q_i q_j}{r_{ij}} \quad (4.12)$$

where  $q_i$  and  $q_j$  are the partial atomic charges on atoms  $i$  and  $j$  separated by a distance  $r_{ij}$ ,  $\epsilon_0$  is the permittivity of free space and  $\epsilon_r$  is the relative dielectric constant, that is a measure of the resistance encountered when forming an electric field in a medium. Normally  $\epsilon_r = 1$  is the standard choice for MD simulations of liquids. Larger values of  $\epsilon_r$  can be used to approximate the dielectric effect of intervening solute or solvent atoms in solution. The point-charge model has serious deficiencies: electrostatic potentials are not always accurately reproduced and non polarizable models do not allow the charges to change as the molecular geometry changes, even though they should. Only pairwise interactions are considered, but even though electrostatic interactions can actually change by the presence of a third body (induction or "polarization" effects). Electrostatic potentials can be more accurately reproduced by allowing the presence non-atom-centered charges. For example this is commonly done to represent the anisotropy in a potential caused by lone pairs on oxygen atoms<sup>[48]</sup>. Another method is to add point dipoles, quadrupoles, etc. However, this does not yet allow the electrostatic variables to change as a function of geometry or to respond to electrostatic potentials generated by nearby atoms, for which the use of polarizable force-fields is required.<sup>[49]</sup>

#### 4.4.2 Lennard–Jones

The Lennard-Jones potential is a common way of representing the London dispersion forces between atoms or molecules in a fluid as well as

their steric repulsion. The force associated with this potential is weakly attractive at long distances, but reverts to a steric repulsion if the molecules get too close. The potential is defined as follow:

$$U_{LJ} = 4\epsilon \left[ \left( \frac{\sigma}{r_{ij}} \right)^{12} - \left( \frac{\sigma}{r_{ij}} \right)^6 \right] = \frac{A}{r_{ij}^{12}} - \frac{B}{r_{ij}^6} \quad (4.13)$$

where  $\sigma$  determines the distance at which the two particles touch with  $U_{LJ} = 0$  and  $\epsilon$  is the strength of the interaction (the well depth) where  $U_{LJ}$  present the minimum value. The first term  $r_{ij}^{-12}$  is responsible for the repulsion at short distance between atoms when they are brought very close to each other. Its physical origin is related to the Pauli principle: when the electronic clouds surrounding the atoms starts to overlap, the energy of the system increases abruptly. The second term  $r_{ij}^{-6}$  is responsible for the attraction at long distance, and gives cohesion to the system. It originates from dispersion forces due to induced dipole-dipole interactions, in turn caused by fluctuating dipoles. A plot of the Lennard-Jones potential is shown in Figure 4.4.

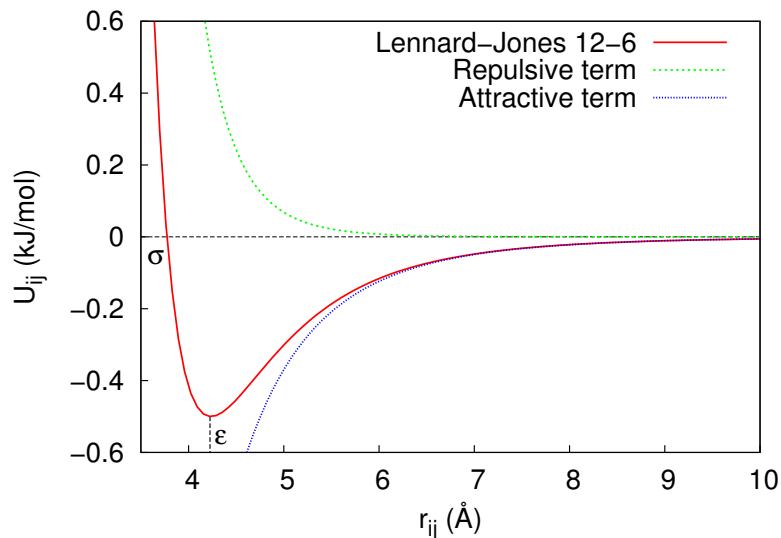


Figure 4.4: Typical LJ 12-6 potential used in MD simulation.

For practical reasons, the Lennard-Jones force is often cut off at a finite distance, often about 10 Å or rather  $3\sigma$ . The effect on the dynamics is small, but the speed-up of the computation can be dramatic. There are cases where only the soft repulsion of the Lennard-Jones potential is necessary (for instance, in simulation of crystals). In such cases, the force is cut off and shifted at the equilibrium distance so there is no attractive force, or simply is omitted the attractive term from the potential .

# Chapter 5

## Polymer-liquid crystals interfaces

### 5.1 Polymer Film interfaces studies

The knowledge of the atomic structure and dynamics of polymer material surfaces is important for several applications. Polymer surfaces have great importance in technologies concerning wetting phenomena (bonding, printing, coating, painting, dusk filters, hard disk drives and uptake of aerosols into the lung etc.)<sup>[50]</sup>. In the last few years polymer films has also been greatly investigated for drug delivery: in these applications, deposited polymer films act as both a coating to modulate surface properties and a reservoir for active therapeutic cargo<sup>[51]</sup>. Moreover A central challenge in polymer science today is creating materials that dynamically alter their structures and properties on demand, or in response to changes in their environment. Surfaces represent an attractive area of focus, since they exert large effects on properties such as wettability, adhesion, optical appearance and bioactivity, enabling pronounced changes in properties to be accomplished through subtle changes in interfacial structure or chemistry<sup>[52]</sup>. In all the above mentioned application, the surface performance is due not only to its chemistry but also to its morphology. It is well known, for example, that the hydrophobic or hydrophilic nature of a surface, in con-

tact with a liquid, is determined not only by chemical composition, but also by its roughness at both nano meter and micro meter scales. Therefore, a knowledge at the atomic level is of paramount importance in order to obtain an in-depth understanding of all these applications. From an experimental point of view, techniques such as sum frequencies generation (SFG), infrared and Raman spectroscopy, inelastic helium atom scattering and first of all Atomic Force Microscopy (AFM) and Scanning Tunnelling Microscopy (STM) have recently allowed to determine the structure at the molecular level and the vibrational dynamics of surfaces<sup>[53]</sup>.

## **5.2 Liquid crystal Displays technology**

The development of computer-related technologies would not have been possible without parallel progress in man-machine interfaces. In particular, liquid crystal display devices (LCDs), characterized by flat panel design, light weight, low power consumption, high information content and large design flexibility, have become a key display technology and polymer-liquid crystal interfaces have a crucial role in their functioning. Current LCD technology started with the invention, in the seventies, of the twisted nematic (TN) LCD.<sup>[54]</sup>

### **5.2.1 Twisted nematic displays**

The twisted nematic effect is based on the precisely controlled realignment of liquid crystal molecules between different ordered molecular configurations under the action of an electric field.

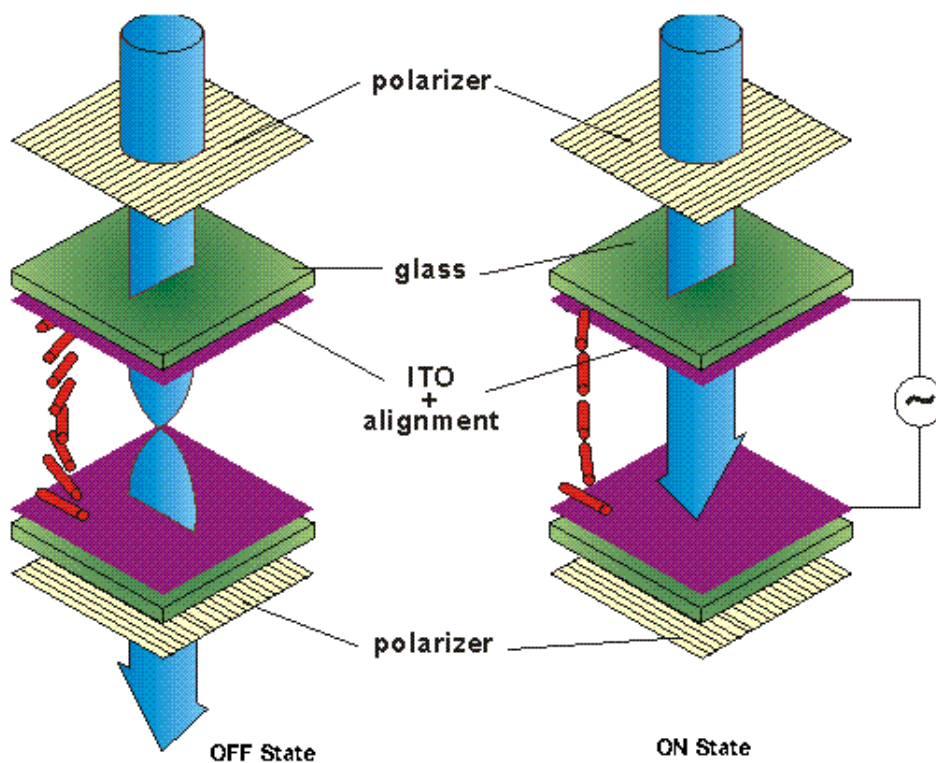


Figure 5.1: A view of a TN liquid crystal cell showing the states in an OFF state (left), and an ON state with field applied (right).

Figure 5.1 shows both the OFF and the ON-state of a single picture element (pixel) of a twisted nematic liquid crystal display. In the OFF state, i.e., when no electrical field is applied, a twisted configuration (helical structure) of nematic liquid crystal molecules is formed between two glass plates, which are separated by several spacers and coated with electrodes, usually made by transparent indium-tin-oxide (ITO). The electrodes themselves are coated with polymer alignment layers that are usually rubbed in one direction, as a result, the LC molecules orient parallel to the rubbing direction. The rubbing directions on the top and bottom substrates are perpendicular to each other, leading to a 90 degrees twist of director from one substrate to the other inside the cell (which is usually 4-10 micrometers thick) when no external field is present. The last essential element of the pixel are two polarizer set at  $90^\circ$  to each other and placed outside the two

glass substrates. If a light source with the proper polarization shines on the back of the LCD, the light will pass through the first polarizer, and into the liquid crystal, where it is rotated by the helical structure. The light becomes then properly polarized to pass through the second polarizers, set at  $90^\circ$  to the first. Conversely in the ON state, i.e., when a field is applied between the two electrodes, the crystal re-aligns itself with the external field. This breaks the twist in the LC and fails to re-orient the polarized light passing through it. In this case, the light is blocked by the second polarizer. A voltage of about 1 V is required to make the crystal align itself with the field, and no current passes through the LC itself. Varying the voltage applied, it is possible to tune the opacity of the pixel. In addition to TN-LCDs, several other LCD operating modes have been introduced and put into practical use during the past 30 years to improve viewing angle dependence. This led to the development of in-plane switching<sup>[55]</sup>, multi-domain vertical alignment<sup>[56]</sup>, and optically compensated birefringence technologies<sup>[57]</sup>. Despite their differences, all LCDs operate with polarized light and by the alignment of LC molecules at the display substrates in one of the two switching states of the display. The specific molecular configuration of a field-effect display enables voltage-induced reorientation of its LC molecules resulting in a change in optical appearance. Display operating modes are characterized by the boundary alignment geometry, the azimuthal and polar surface interactions of the respective LC-directors at the substrates, the type of LCs used and the properties of the bulk LC material. Another key parameter is the pretilt angle, which is the angle formed between the liquid crystal molecules and the surface of alignment film. Precise control and stability of both uniaxiality and pretilt over the entire display substrate under all driving conditions are prerequisites for proper display operation.<sup>[58]</sup>

## 5.3 Rubbing and LC alignment

The uniaxial alignment of LCs was mainly achieved by a rubbing process. During this treatment, the surfaces of polymer coated display substrates are rubbed in one direction by a rotating cylinder covered with a rubbing cloth. Enhanced display quality and increased substrate size has resulted, however, in the rubbing process meeting both its technical and economic limits and thus the need for alternative aligning technologies<sup>[59]</sup>. Serious drawbacks of the rubbing process include:

1. rubbing with high-speed rollers degrades the rubbing cloth, requiring frequent cloth replacement and precise and costly readjustment of the rubbing equipment;
2. shaved-off polyimide flakes and cloth wastes result from rubbing;
3. rubbing the insulating aligning layer on top of thin-film transistors (TFTs) causes damage to active TFT-LCD substrates by static discharge;
4. rubbing traces on the surface of alignment layers degrade display contrast.

Indeed, since glass substrates were first rubbed with a cloth in 1911 to align nematic LCs in a study of the optical anisotropy of such LCs, many rubbing processes have been suggested.<sup>[2]</sup> In particular, rubbing of coated and uncoated surfaces with a cotton, nylon or rayon cloth in one direction was shown to be an efficient and inexpensive alignment method, and has been widely adopted by the LCD industry. LC alignment layers were initially composed of poly(vinyl alcohol) (PVA), which was gradually replaced by polyimides (PIs) since 1982. The main reasons for replacement are the hygroscopic nature, the weak heat-tolerance and the poor voltage holding ratio of PVA. During the rubbing process, microgrooves are generally created on the polymer film surface and, at the same time,

the polymer chains at the film surface are stretched by rotation of the cylinder. This results in the uniaxial alignment on the rubbed film surface of LC-molecules at a pretilt angle, depending on the rubbing pressure, rotation speed, type of polymer coating used, layer annealing conditions, and type of LCs used in the display. Basically, LC alignment involves two aligning directions: uniaxial planar (homogeneous) and vertical (homeotropic) to the display substrate. Most studies have shown that LCs on the surface of the rubbed polymer film layer are aligned parallel to the direction of rubbing. In these systems, microgrooves are generated on the film surface along the rubbing direction and also the polymer chains are stretched in this direction. Since both the parallel aligned microgrooves (i.e. the topographical effect) and the polymer chains at the film surface may play a role in the LC alignment, it is not easy to quantify the effect of each contribution<sup>[58][59]</sup>.

## 5.4 Clues on LCs alignment on polymers

Much effort has been made to understand whether micro-grooves or polymer chain orientation causes LC alignment or in other words whether the origin of the alignment is as a specific/physical or specific/chemical. The following findings suggest that LC alignment probably is dominated by the molecular interaction between the alignment layer and LC molecules rather than by interaction with the microgrooves:

1. rubbing of alignment polymer layers, such as PVA, nylon 6/6 and poly(ethylene terephthalate) (PET), in one direction, followed by rubbing in the perpendicular direction, showed that the direction of LC alignment was always parallel to the second rubbing direction, despite the microgrooves being perpendicular to each other<sup>[60]</sup>;
2. rubbed conventional PI films show alignment of LC molecules parallel to the rubbing direction with the parallel oriented polymer chains and microgrooves, but this LC alignment ability is completely lost

when very thin Pt-Pd layers (about 3 nm) were deposited on their surfaces, despite the continued presence of microgrooves, again indicating that LC alignment is dominated by interactions with parallel oriented PI polymer chains rather than with parallel microgrooves<sup>[61]</sup>;

- poly(4, 4'-(9, 9-fluorenyl)diphenylene- cyclobutanyl-tetracarboximide) (CBDA-FDA PI) films showed LC alignment perpendicular to the rubbing direction with microgrooves and polymer main chains running parallel, whereas poly(p-phenylene 3, 6 -bis(4 -(n-alkyloxy)phenoxy)pyromellitimide) (PMDA-PDA PI) films with meandering microgrooves running perpendicular to the rubbing direction showed alignment of LC molecules parallel to the rubbing direction with the polymer main chains oriented in parallel. In particular, the fluorenyl side groups in CBDA-FDA PI showed stronger interactions with LCs than the other chemical components<sup>[62]</sup>. (See figure 5.2).

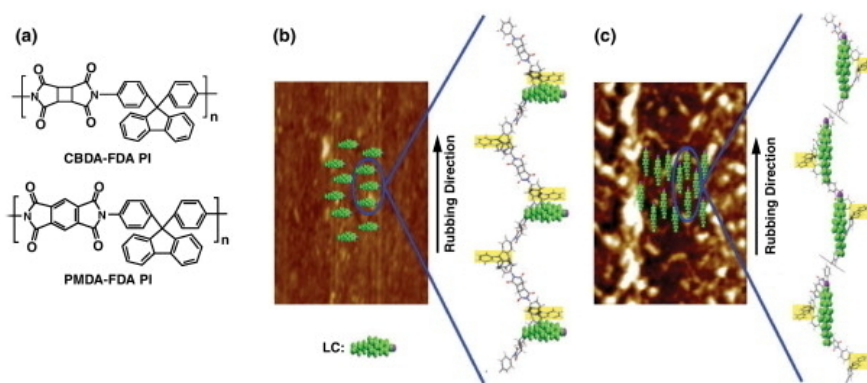


Figure 5.2: Chemical structures of CBDA-FDA and PMDA-FDA PIs (a); AFM height image of a rubbed CBDA-FDA PI (b) and PMDA-PDA PI (c) with a schematic configuration model of PI chains at the rubbed film surface induced LC alignment.<sup>[62]</sup>

For all of the above mentioned polymers, the LCs had relatively high azimuthal anchoring energies,  $\gg 1 \times 10^{-6} J/m^2$ .

### 5.4.1 Polystyrene - liquid crystal studies

Rubbed PS films constitute a good LC alignment layer system to clearly demonstrate the effect of microgrooves in LC alignment. LCs alignment driven by microgrooves generated on a rubbed polymer film (i.e. topographical effect) it is more likely to be found for polymers with weak molecular interactions with LC molecules. LCs on rubbed polymer surfaces are anchored with very low energy, as in the case of polystyrene (PS), ranging from  $4 \times 10^{-8}$  to  $3 \times 10^{-7} J/m^2$  (depending on the PS molecular weight, which affects microgroove formation, higher molecular weight PS films exhibited higher azimuthal energies), present limited alignment stability<sup>[63]</sup>.

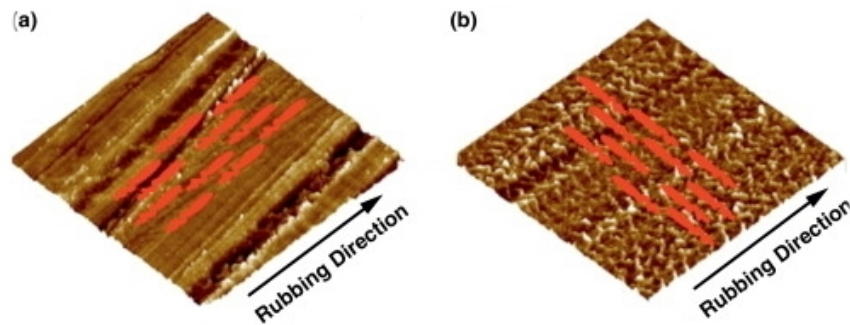


Figure 5.3: AFM height images of a rubbed film of PS with  $\bar{M}_w < \text{ca. } 10000$  (a) and  $\bar{M}_w > \text{ca. } 10000$  (b) with a schematic representation of LCs alignment<sup>[64]</sup>.

From experimental and theoretical studies<sup>[65][66]</sup>, the rubbed PS films exhibited molecular orientations independent of molecular weight: the vinyl backbones were preferentially oriented along the rubbing direction while the planes of the phenyl side groups were oriented nearly perpendicular to the rubbing direction with para-directions that were positioned nearly normal to the film plane (see Figure) 5.3. However rubbed PS films of average molecular weight  $\bar{M}_w < \text{ca. } 10000$  show the development of sub-microscale grooves along the rubbing direction, whereas rubbed PS films of  $\bar{M}_w > 10000$  show the development of meandering groove-like structures perpendicular to the rubbing direction<sup>[64]</sup>

The direction of LC alignment always coincided with the direction of orientation of the generated submicroscale grooves.<sup>[64]</sup>

Three factors are believed to be possible causes of the LCs alignment:

1. the interactions of LCs with the oriented vinyl main chains;
2. the interactions of LCs with the oriented phenyl side groups;
3. the anisotropic interactions of LCs with submicroscale grooves.

In PS film, none of these three anisotropic interactions between the LCs and the rubbed surface seems to be dominant in the determination of LC alignment. Therefore, the alignment of LCs appears to be governed by the cooperative interaction of the oriented main chain segments and side groups with submicroscale grooves, whose directionally anisotropic interactions compete in aligning LC molecules<sup>[64]</sup>.

#### **5.4.2 Polymethyl-methacrylate - liquid crystal studies**

Another important phenomenon to consider for liquid crystal alignment is the formation of friction charges induced by the rubbing process. For polymers like PMMA, which present low anchoring energy  $\leq 5 \times 10^{-6} J/m^2$ , well defined surface charge domains oriented along the rubbing direction were observed, with the electrical potential increasing with the number of rubbings. For polymers like polyvinyl alcohol (PVA), no induced charge domains were observed. This can be explained considering the chemical structure of the polymer. The hydroxyl groups of the PVA polymeric chains are good charge conductors, therefore the charges formed by the rubbing process can leak out of the surface, instead PMMA does not contain OH groups and therefore charged species may localize on the surface for a long time. AS theoretically suggested, the coupling of the electric field generated by the surface density of charges with the nematic medium can affect the bulk orientation of the director by distorting the director profile

near the surface. For a medium with positive dielectric anisotropy (which is the case for 5CB), in a planar configuration of the director the electrostatic potential seems to destabilize the bulk alignment<sup>[67,68]</sup>.

## Chapter 6

# Simulation study of the Polymer-LC interface

The past few decades have seen a dramatic increase in the use of atomistic simulations as a support for the experimental techniques in order to address problems in materials science. The growing popularity of this type of simulations arise from the fact that the quality of interatomic potentials has been improving for many systems, and also from the continuously increasing computational power of modern supercomputers<sup>[69]</sup>. Here, we wish to reach an in-depth knowledge of LCs alignment induced by polymers surfaces and understand the mechanism governing LC alignment. Several PMMA and PS samples were interfaced with the well known and studied 5CB liquid crystal, and studied through MD simulations. The application of polymeric surfaces in LCD technologies has motivated several studies concerning polymer-LC, both experimental and theoretical are available in literature, but only few experimental and theoretical works on polymer-liquid crystals interfaces<sup>[66]</sup>. We specifically focused on PS and PMMA polymers since their interface with the liquid crystalline phase has already been well studied in literature<sup>[64,65,70]</sup>, like described in the previous chapter.

## 6.1 Methods and simulation details

The first step of this simulation study has been the preparation of the surfaces that were later used to study the effect of the polymeric interface on the liquid crystal phase.<sup>[70]</sup> Polymeric chains have been modelled at full atom level of detail using a customized AMBER94 molecular mechanics force field (FF)<sup>[71]</sup>, previously employed in the study of the interaction between pentacene and PS/PMMA<sup>[72]</sup>. Each macromolecule has been built by linking 50 monomers in the reacted form (without the terminal hydrogen), obtaining isotactic polymers. Once the polymeric chains were created, we packed them to obtain the following surfaces: **1.** amorphous PS surface consisting of 60 chains arranged in a disordered fashion (PSi); **2.** ordered PS surface, consisting of 60 elongated chains arranged in a parallel fashion (PSo); **3.** amorphous PMMA surface consisting of 72 chains arranged in a disordered fashion (PMMAi); **4.** ordered PMMA surface, consisting of 72 elongated chains arranged in a parallel fashion (PMMAo). The number of chains constituting the samples has been estimated using experimental densities values<sup>[73]</sup> in order to obtain surfaces roughly  $10^4$  Å<sup>2</sup>-wide and 50 Å-thick. Packing of amorphous polymers **1.** and **3.** was achieved by applying a high pressure to the samples (1000 atm). Once the volume of the simulation box reached a constant value, surfaces were then equilibrated at the constant pressure of 1 atm first at 700 K, a temperature well above the glass transition temperature  $T_g$  (351 K for PS and 314 K for PMMA<sup>[74,75]</sup>) and then at 300 K. Ordered samples **2.** and **4.** were built starting from a single elongated polymeric chain, which was replicated regularly in space to form a bulk sample. The chain elongation was performed by applying two equal forces, in opposite direction ( $1 \text{ kcal mol}^{-1} \text{ \AA}^{-1}$ ) to the external carbon atoms of the terminal monomers of each chain. Stretching forces on the chains were applied during the packing process that, as for the amorphous case, was performed at high pressure. After compression, all samples were equilibrated for about 50 ns at 300

K until they reached a constant, equilibrium thickness. Pressure was controlled through Langevin piston in order to keep the x and y axis of the cell at a constant value during the compression, a value that was imposed to be 100 Å for both sides, thus maintaining the square section of the cell<sup>[76]</sup>. Once the desired surfaces have been prepared (see snapshot in Figure 6.1 for the snapshots), we proceeded with setting up the LC-polymer interface simulations by adding 5CB on top of each polymeric surface. Three samples with 1000 and 3000 molecules of 5CB were built for each surface, for a total of 8 starting configurations (see Figure 6.2 for the snapshots of ordered and amorphous PS interfaces with 3000 5CB molecules). 5CB molecules were modelled at UA level of detail using a AMBER-OPLS force field<sup>[71]</sup>, which was previously tuned in-house to reproduce the experimental nematic-isotropic transition temperature of n-alkyl cyano biphenyls with 5 to 8 carbon atoms in the linear alkyl chain<sup>[77]</sup>. Simulations were run in NPT conditions using NAMD<sup>[78]</sup> with multiple step integration: bonded, Van Der Waals and electrostatic interactions were calculated every 1, 2 and 4 fs respectively. Three dimensional periodic boundary conditions were used in all simulations and long range electrostatic interactions were computed with the Particle Mesh Ewald method<sup>[79]</sup>. Temperature was kept constant at 300 K through velocity rescaling. All simulations were equilibrated for at least 50 ns, while production time ranged from 100 ns to 160 ns.

## 6.2 Results and discussion

In this section the most relevant computational observables for LC-polymer systems are reported and discussed. The choice of running simulations with three dimensional PBC determines the existence of two 5CB-polymer interfaces at the opposite of the simulation box. In most of the following plots, the origin of the z axis is arbitrary set in the middle of 5CB film, thus locating the two interfaces at the positive and negative end of the graphs.

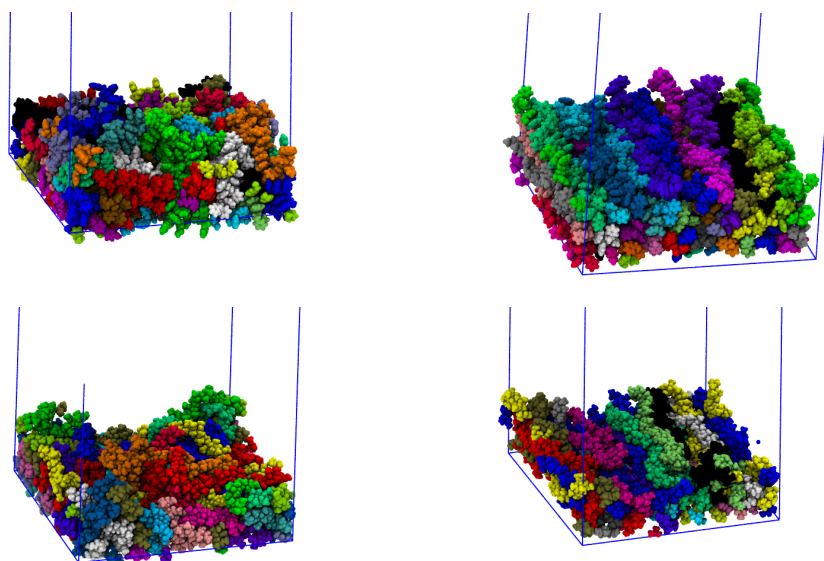


Figure 6.1: Top: surface snapshots of **1.** PSi (Left) and **2.** PSo (right) surfaces. Bottom: snapshots of **3.** PMMAi (left) and **4.**PMMAo (right) respectively.

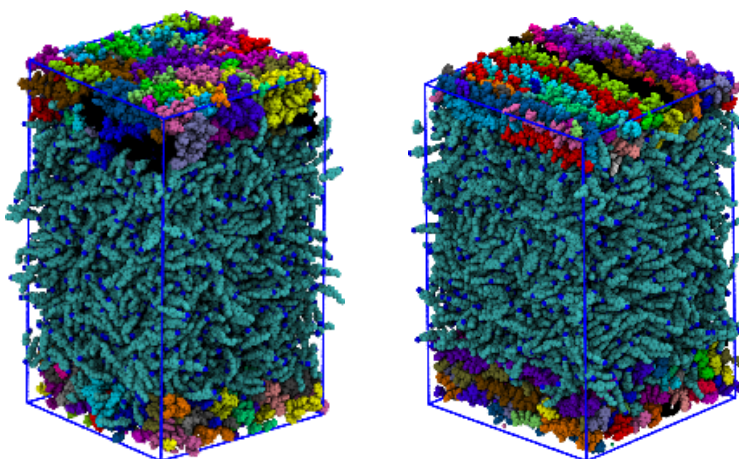


Figure 6.2: Snapshots of the starting configurations composed by PS surfaces **1.** and **2.** (left and right) and the liquid crystal phase comprising 3000 molecules of 5CB. Every single polymer chain is represented with a different color.

Table 6.1: Polymer and 5CB bulk densities for different samples with 3000 molecules of 5CB.

sample	Polymer density (g/cm <sup>3</sup> )	5CB bulk density (g/cm <sup>3</sup> )
PMMA <sub>o</sub>	1.07 ± 0.07	1.02 ± 0.01
PMMA <sub>i</sub>	1.04 ± 0.09	1.02 ± 0.01
PS <sub>o</sub>	0.99 ± 0.06	1.02 ± 0.01
PS <sub>i</sub>	0.99 ± 0.07	1.02 ± 0.01

### 6.2.1 Density profiles

A preliminary characterization of the interfaces can be performed by plotting the mass density profile along the  $z$  axis of the box,  $\rho(z)$ , which is easily accessible to simulations. The mass density as a function of  $z$  is calculated by partitioning the simulation cell into bins along the  $z$ -direction, with a bin thickness of 2.5 Å, and summing the masses of atoms in each bin per partitioned volume. The  $\rho(z)$  profiles, reported in Figure 6.3, show two nearly symmetric LC/polymer interfaces for all samples. The LC bulk region can be found from -20 to 20 Å for samples with 1000 5CB molecules and from -60 Å to 60 Å for samples with 3000 5CB molecules. Distinguishing the polymer bulk phase from the interfaces can be tricky due to the relative subtlety of the polymer films. In fact, unlike solid surfaces (such as the silica case<sup>[5,6]</sup>) polymers, given their organic nature, form more rough, soft and deformable surfaces. Using a linear extrapolation on the smoother densities profiles of bigger samples, it was found an interface thickness of 1.5 nm and 2 nm for PS and PMMA respectively. To compute the LC liquid density reported in Tab 6.1, densities were arithmetically averaged in the bulk region. The calculation of polymer densities is less accurate, as the coordinates of the range in which the bulk polymer is found can be hard to be define. The density of 5CB corresponds to that measured at room temperature reported in literature (1.02 g/cm<sup>3</sup>)<sup>[80]</sup>. Slight differences were found for polymer simulated densities compared to experimental ones i.e. 1.16-1.20 g/cm<sup>3</sup> for PMMA, 1.04-1.09 g/cm<sup>3</sup> for PS<sup>[73,80]</sup>.

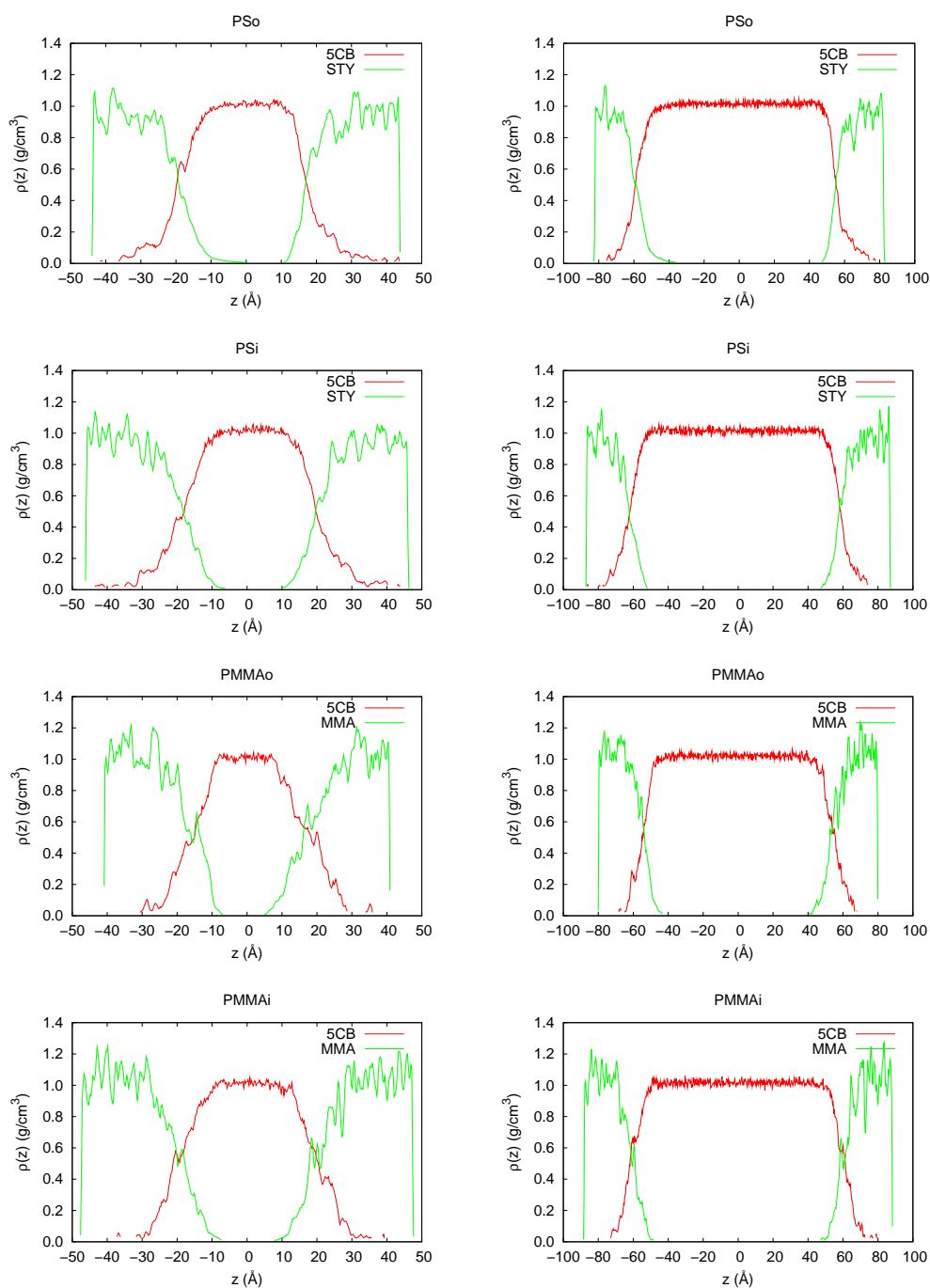


Figure 6.3: Density profiles  $\rho(z)$  along the  $z$  coordinate of the simulation box of PSo, PSi, PMMAo and PMMAi for samples with 1000 (left column) and 3000 (right column) molecules of 5CB.

Table 6.2: Roughness of top (negative z values) and bottom (positive z values) surfaces for samples with 3000 molecules for starting (S-top and S-bottom) and final configuration (F-top and F-bottom).

Sample	S-top (Å)	S-bottom (Å)	F-top (Å)	F-bottom (Å)
PMMAo	4.34	4.62	4.50	5.37
PMMAi	5.07	4.97	5.47	4.20
PSo	4.04	3.65	7.61	4.41
PSi	3.15	2.50	5.16	5.00

## 6.2.2 Characterization of polymer surfaces

The surface film roughness can be quantified by using the standard deviation of the height, defined as:

$$W = \left\langle \sqrt{\frac{1}{N^2} \sum_{i=1}^N (h_i - \bar{h})^2} \right\rangle \quad (6.1)$$

where  $N^2$  is the number of grid points on the surface (in the present case, we used  $N = 10^4$ ) and  $h_i(t)$  and  $\bar{h}(t)$  are the heights of point  $i$  at time  $t$  and the average height at time  $t$ , respectively. Surfaces were probed using a cubic tip of side 4.5 Å, in analogy with the experimental AFM technique. The average roughness for the top and bottom sides of the film surface was calculated and both values are reported in Table 6.2, whilst in Figure 6.4 the topography of ordered and disordered surfaces can be observed. As shown in Table 6.2, the roughnesses are at least ten times lower for all the samples compared to experimental values, which range between 2 and 5 nm for PS<sup>[81]</sup> and between 3 and 4 nm for PMMA<sup>[82]</sup>, depending on the polydispersity and surface preparation. It can also be noticed that the initial PS roughness increases during the simulation, due to the partial solvation of few chains especially in PSo top surface (see Figure 6.5). Partial solubility of PS in 5CB at 300 K is also found experimentally, as reported in reference<sup>[83]</sup>.

It is also worth characterizing the conformation of the polymer chains in the different samples. For instance, can describe the conformation of a

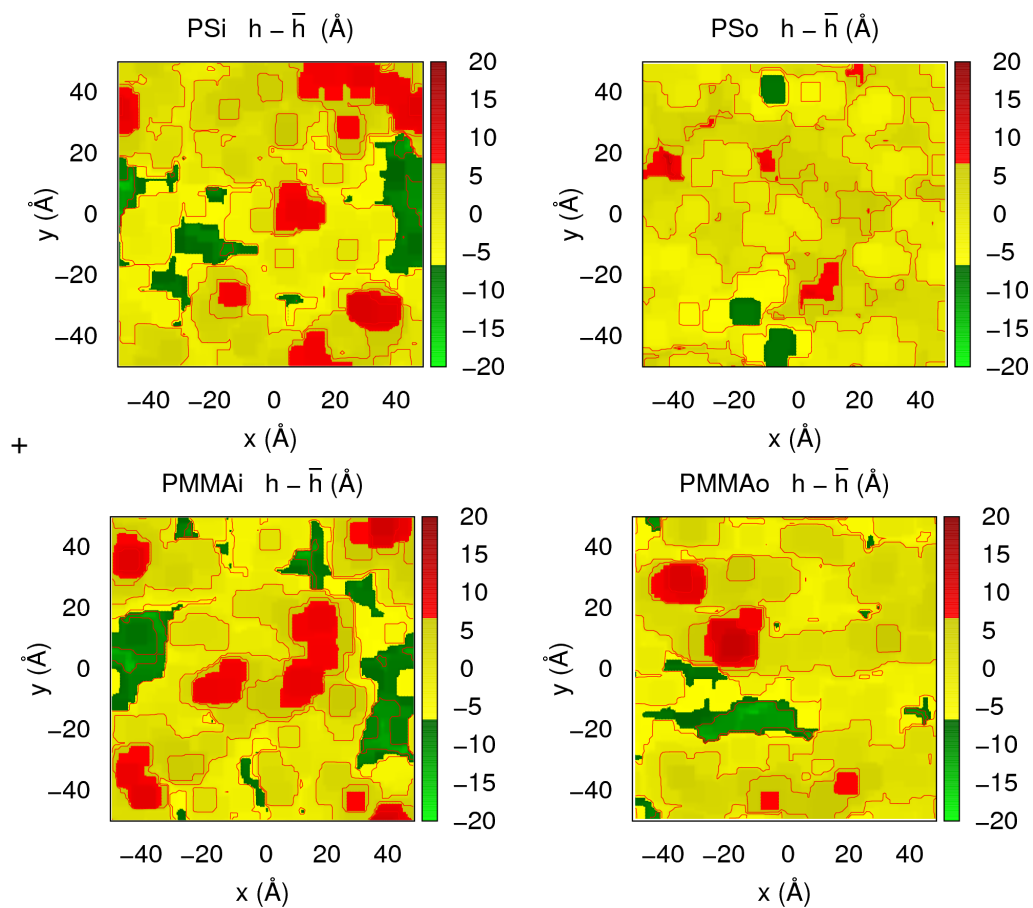


Figure 6.4: Topography maps, averaged on the last 2 ns of the simulation trajectory, for PS and PMMA top surfaces for samples with 3000 5CB molecules.

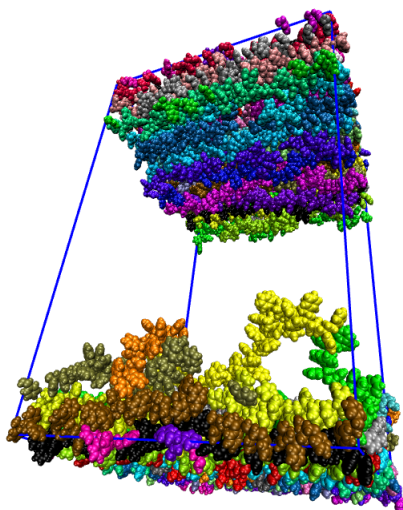


Figure 6.5: Snapshot of partial dissolution of some chains in PSo sample with 3000 molecules.

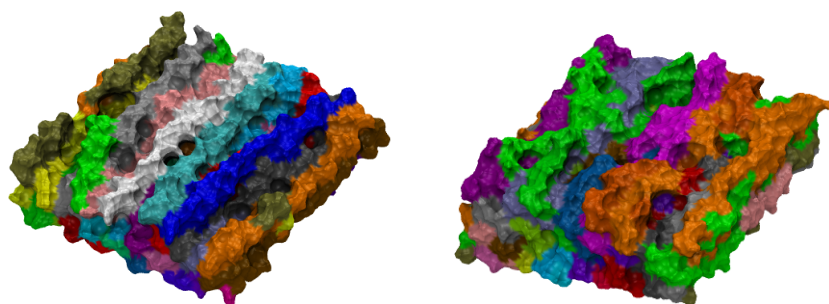


Figure 6.6: Solvent-excluded surface for samples PSo (left) and PMMAo (right) with 3000 5CB molecules.

polymer by giving the positions of its backbone atoms. The positions of the remaining atoms then usually follow by simple chemical rules. So, suppose we have  $N$  monomers, with  $N$  center of mass position vectors:

$$\mathbf{r}_1, \mathbf{r}_2, \dots, \mathbf{r}_N \quad (6.2)$$

Much of the static and dynamic behavior of polymers can be explained through models which are surprisingly simple. For example, it can be measured the end-to-end vector, defined as:

$$\mathbf{R} = \mathbf{r}_N - \mathbf{r}_0 \quad (6.3)$$

The norm of the end-to-end vector is called the end-to-end distance. An alternative measure of the size of a polymer chain is provided by its *radius of gyration*,  $R_g$ , which can be measured by light scattering experiments and it is defined by:

$$R_g^2 = \frac{1}{N} \sum_{i=1}^N (|\mathbf{R}_i| - \langle |\mathbf{R}| \rangle)^2 \quad (6.4)$$

where  $\mathbf{R}_i$  is the position of the single monomers and  $|\mathbf{R}|$  is the mean position of the monomers. A small radius of gyration or a small end-to-end distance indicates that the polymer is relatively compact, meaning that throughout its trajectory the polymer spends most of its time as a folded structure. In Figure 6.7, the probability distribution of the value of the end-to-end distance is reported. The distributions of the ordered samples are narrower and shifted towards higher values than disordered ones. Values of the end-to-end distance reported in Table 6.3 show that ordered chains are stretched over the full length of the box, as it can be also seen in Figure 6.1. In Table 6.3 are also reported values of the gyration radius of polymer chains: for disordered samples they are similar to that found experimentally for PS (19.3 Å for 51-monomers chains in cyclohexane at 34.5 °C)<sup>[84]</sup> and PMMA (16- 25 Å for 31-71-monomers chains in acetone

Table 6.3: End-to-end distance and gyration radius for polymer chains in samples with 3000 5CB molecules.

sample	End to end distance (Å)	Gyration radius (Å)
PMMAo	$102.5 \pm 3.9$	$27.1 \pm 1.8$
PMMAi	$46.3 \pm 12.4$	$19.8 \pm 2.6$
PSo	$93.9 \pm 10.3$	$28.7 \pm 2.2$
PSi	$36.4 \pm 13.4$	$18.9 \pm 2.8$

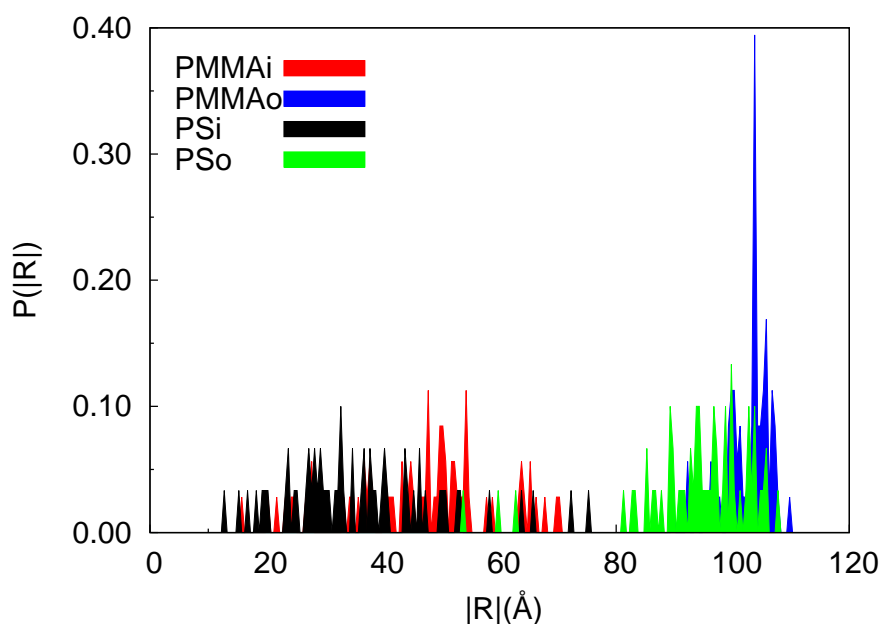


Figure 6.7: Probability distribution of the end-to-end distance  $P(|R|)$  for PMMA and PS samples with 3000 molecules of 5CB.

at 25 °C)<sup>[85]</sup>.

### 6.2.3 Molecular organization of 5CB

Almost any surface can cause the director  $\mathbf{n}$  of an LC phase, to orient in a specific direction in proximity of the interface. There are three main types of the LC director alignment near a solid wall or at the free surface. These are homeotropic, planar and tilted orientations. The surface which is in contact with mesophase is usually considered to be flat on the

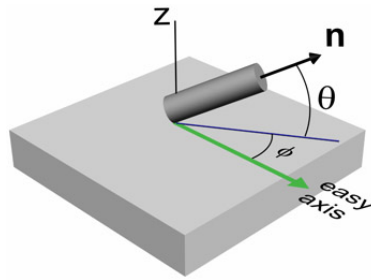


Figure 6.8: Schematic representation of LC alignment on a planar surface.

microscopic scale, and the position of the director in its proximity is determined by polar or tilt angle  $\theta$  and azimuthal or twist angle  $\phi$  (see Figure 6.8). When the director  $\mathbf{n}$  is oriented homeotropically, the polar angle  $\theta$  is  $90^\circ$ . The director with planar orientation lies in the plane of the surface or phase separation border. In this case two possible orientations exist: one, homogeneous planar orientation, when the director is oriented uniformly over the surface and  $\phi$  is fixed; another, heterogeneous planar orientation, when the orientation of the director is not uniform over the surface and  $\phi$  has different fixed values in different points of the surface. In case of a tilted orientation,  $\theta$  is fixed and  $\phi$  is arbitrary. The preferred direction of the director at the surfaces set by the alignment is called *easy axis*.

The presence of an orientationally ordered phase can be easily identified by monitoring a suitably defined *orientational distribution function* (ODF). If 5CB molecules were approximated by uniaxial objects with orientation axis  $\mathbf{u}$  (which is of course strictly not true, but reasonable in describing such complex mesogens with a minimal model) and we assume the liquid crystal to be cylindrically symmetric around a director  $\mathbf{n}$ , the ODF reduces to  $f(\beta)$ , the probability of finding one molecule at a certain angle  $\beta$  from the director.

The ODF can be expanded in a series of Legendre polynomials  $P_L(\cos \beta)$ :

$$f(\beta) = \sum_{L=0}^{\infty} \frac{2L+1}{2} \langle P_L \rangle P_L(\cos \beta) \quad (6.5)$$

with the first terms of the series being:

$$P_0(\cos \beta) = 1 \quad (6.6)$$

$$P_1(\cos \beta) = \cos \beta \quad (6.7)$$

$$P_2(\cos \beta) = \frac{3}{2} \cos^2 \beta - \frac{1}{2}, \quad (6.8)$$

and with the distribution  $f(\beta)$  normalized so that  $\int_0^\pi f(\beta) \sin \beta d\beta = 1$ .

Of course if the symmetry of the phase requires it, a more general expression of the ODF can be written, considering all the three Euler angles  $\alpha$ ,  $\beta$ ,  $\gamma$ , and expanding the ODF in terms of Wigner matrix elements. Limiting ourselves to the simplest uniaxial case, the average order parameter  $\langle P_1 \rangle$  is relevant in case of polar order, for example for polar molecules in contact with a surface, and ranges from -1 (antiparallel) to 1 (parallel orientation). The calculation of this function requires to set up an ordering matrix  $\mathbf{Q}(t)$ , summing over all  $N$  molecules of the sample:

$$\mathbf{Q}(t) = \frac{1}{2N} \sum_{I=1}^N [3\mathbf{u}_I(t) \otimes \mathbf{u}_I(t) - \mathbf{I}], \quad (6.9)$$

where  $\mathbf{u}_I(t)$  is the chosen reference molecular axis and  $\mathbf{I}$  is the identity matrix. The instantaneous order parameter  $P_2(t)$ , which corresponds to the value of  $P_2$  for each configuration, can be obtained from the eigenvalues  $\lambda_-(t) < \lambda_0(t) < \lambda_+(t)$  of the  $\mathbf{Q}$  matrix. According to the most common convention,  $P_2(t)$  corresponds to the largest eigenvalue, which is to say  $P_2(t) = \lambda_+$ , and once a sufficiently long trajectory is available, the time average  $\langle P_2 \rangle$  is calculated<sup>[86]</sup>. The director  $\mathbf{n}$  instead is calculated as the eigenvector corresponding to the eigenvalue  $\lambda_+$ .

The second rank order parameter  $\langle P_2 \rangle$  is instead commonly used to characterize the average degree of alignment of a liquid crystal phase and the transition from a disordered to an orientationally ordered phase, such as the isotropic-nematic one. This order parameter assumes again a value of 1 for perfectly parallel molecules, 0 for an isotropic distribution of orien-

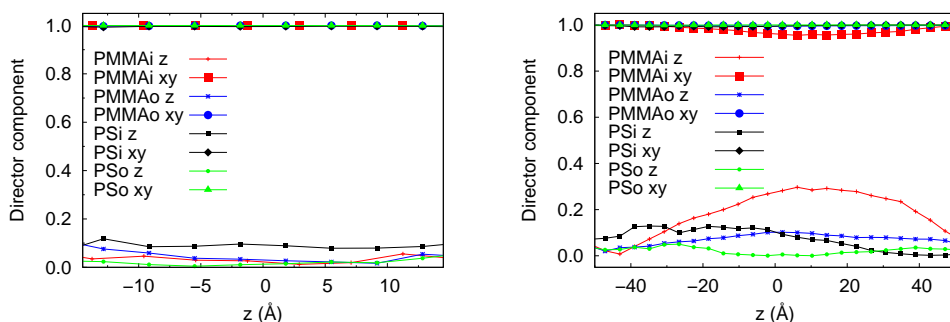


Figure 6.9: xy (planar) and z (perpendicular) director component for sample with 1000 (left) and 3000 (right) molecules of 5CB.

tations, and -0.5 for molecules perpendicular to the phase director. The special orientation in which  $P_2$  is equal to zero but the system is still ordered is named “magic angle” (about 54.74 degrees).

In Figure 6.9 are shown z and  $xy = (\sqrt{1 - z^2})$  director components for 5CB molecules calculated using slabs of 0.5 nm. It can be noticed that in all studied samples molecules show a preferential planar alignment, with the xy component being always close to unity through the whole LC phase. This is in agreement with experimental studies: in particular, PMMA shows planar alignment<sup>[87]</sup> and PS films have also been found to align LCs perpendicularly to the rubbing direction with zero pretilt angle<sup>[88]</sup>.

In Figure 6.10 the x and y components of easy axis of the bottom and top surfaces of different samples are reported. Interestingly, ordered surfaces show similar x and y component at both interfaces, while disordered samples display different director orientations.

Moreover, while in PMMA ordered surfaces 5CB molecules are oriented along the polymer chains (x axis), in PS, they tend to be oriented perpendicularly (see Figure 6.11).

The Figure 6.12 shows the polar and azimuthal angles of the 5CB director along the z axis of simulation box. From the polar angle, it can be seen that 5CB molecules are only slightly tilted with respect to the surface in all samples and in particular on ordered surfaces they are less tilted than

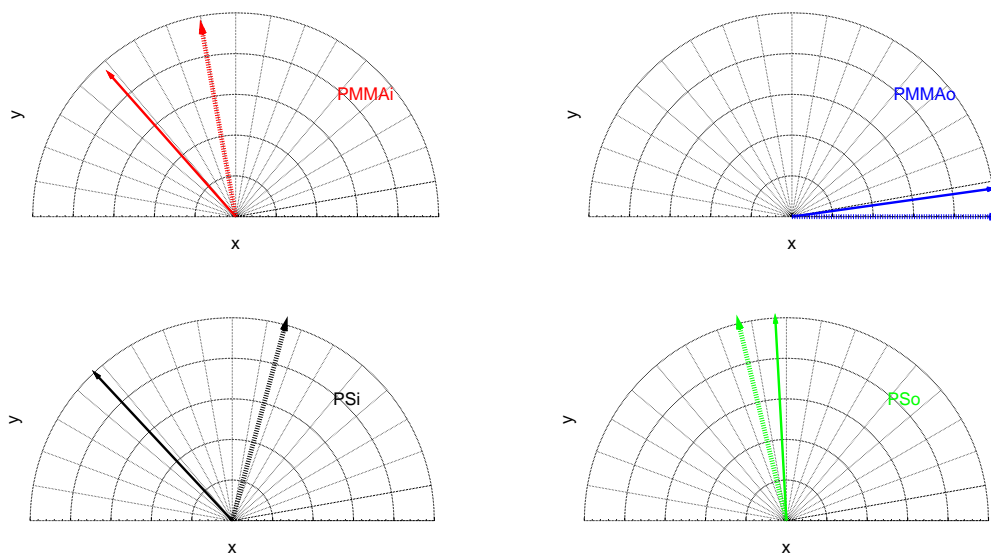


Figure 6.10: Easy axis of 5CB at the bottom surface (continuous arrows), and at the top surface (dotted arrows). Top: PMMAi (left) and PMMAo (right). Bottom: PSi (left) and PSo (right). Only the x and y components are shown, with the out of plane tilt being comprised between 0 and 8 degrees.

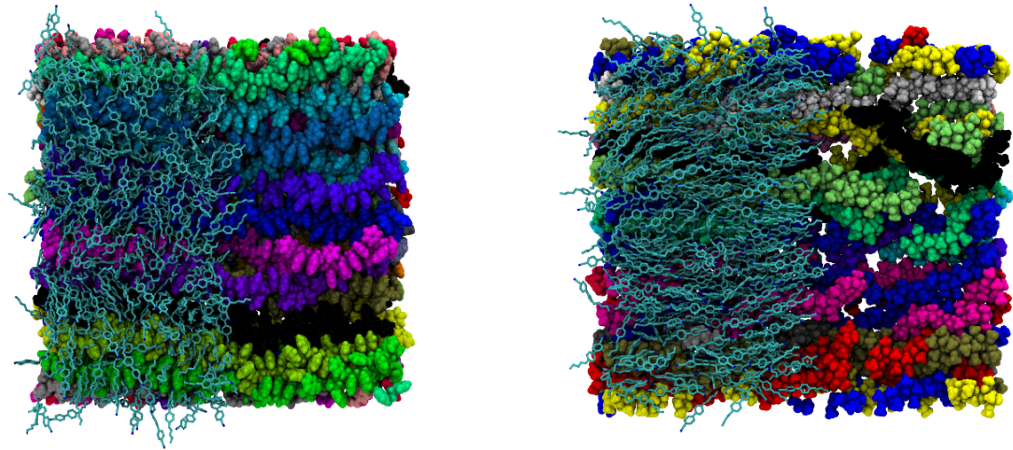


Figure 6.11: Snapshot showing the different planar orientation of 5CB wireframe molecules PS (left) and PMMA (right) ordered samples with 3000 molecules.

on the respective disordered ones. From the trend of the azimuthal angle, instead, as a consequence of the different top and bottom orientation of the easy axis, in disordered samples are twisted in the xy plane between surfaces while in ordered samples they are almost uniformly aligned.

In Figures 6.13 the instantaneous orientational order parameter  $P_2$  of the 5CB liquid crystal is shown. Low values of  $P_2$  (around 0.2-0.3, Table 6.4) were found for all samples with exception for the PMMAo with 1000 and 3000 5CB molecules, that seems to show a nematic behaviour, with a  $P_2$  value around 0.45. The PSo does not show higher values of  $P_2$  with respect to PSi and only a weak increase of order was found in the biggest samples.

In Figure 6.14,  $\langle P_2 \rangle$  as a function of z position in the simulation box is reported. Again, it can be observed that PMMAo is the sample featuring the most ordered LC phase, confirming what already seen in the Figure 6.13. All samples present lower values of  $\langle P_2 \rangle$ , in close to the surfaces

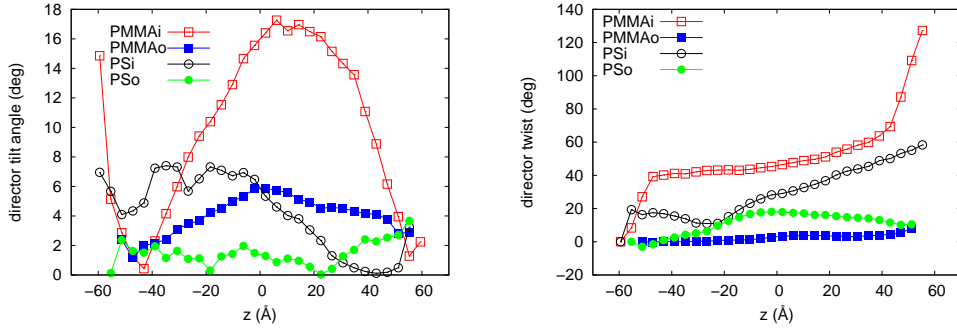


Figure 6.12: Polar (left) and azimuthal (right) angles of the LC phase director for samples with 3000 5CB molecules.

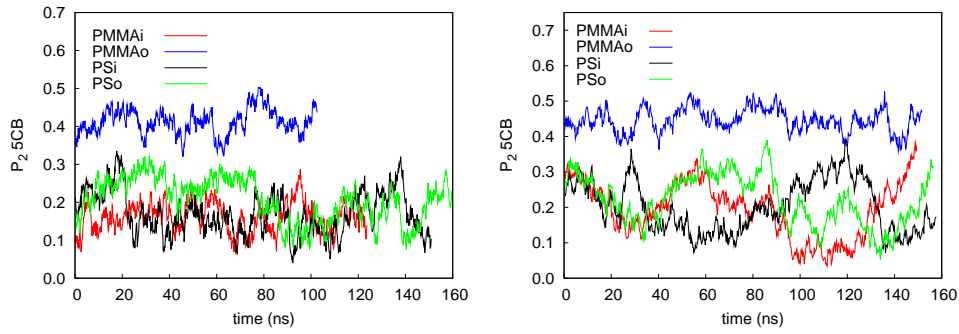


Figure 6.13: Instantaneous values of 5CB  $P_2$  as a function of time for samples of 1000 (left) and 3000 (right) 5CB molecules.

sample	N	$\langle P_2 \rangle$
PMMAo	1000	$0.41 \pm 0.03$
PMMAi	1000	$0.16 \pm 0.04$
PSo	1000	$0.21 \pm 0.06$
PSi	1000	$0.17 \pm 0.06$
PMMAo	3000	$0.45 \pm 0.03$
PMMAi	3000	$0.19 \pm 0.08$
PSo	3000	$0.22 \pm 0.07$
PSi	3000	$0.20 \pm 0.07$

Table 6.4: Average nematic order parameter  $\langle P_2 \rangle$  and its standard deviation for studied samples.

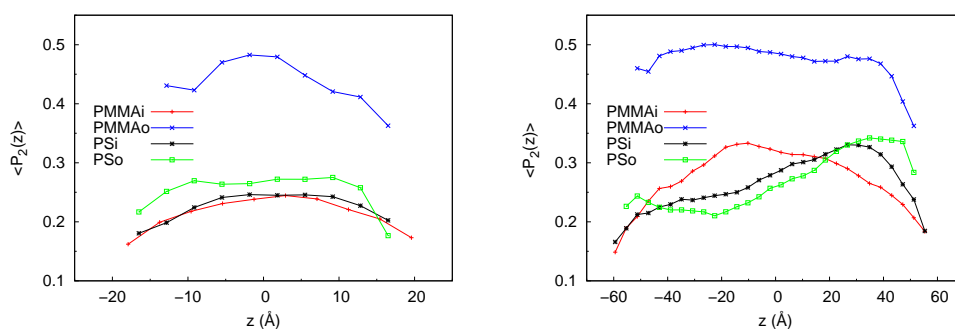


Figure 6.14: Average orientational order parameter  $\langle P_2(z) \rangle$  calculated in 0.5 nm wide slabs along z axis of the simulation box for samples composed by 1000 (left column) and 3000 (right column) 5CB molecules.

than in the middle of the LC film. This is probably due to the diffusion of the 5CB phase in the polymer film. It can also be seen that for the PSo sample, the  $\langle P_2 \rangle$  profile is not symmetric, but values tend to be higher near the bottom surface, which is less rough than the top surface where some chains were partially dissolved (see Table 6.2 and Figure 6.5). Moreover, it can be noticed a slight increase in  $\langle P_2 \rangle$  values with in bigger samples.

In Figure 6.15 instead we report the time evolution of the orientational parameter, calculated in slabs of 0.5 nm along the z coordinate, of the 5CB liquid crystalline phase. As already seen in Figure 6.13, the only sample that seems to manifest a truly nematic behaviour of the liquid crystalline phase is PMMAo. It can be also seen that bigger samples are slightly more ordered than smaller ones (yellow and red regions in Figure 6.15).

Finally in Figures 6.16 the polar order parameter  $\langle P_1 \rangle$  of the liquid crystalline phase for different samples is reported. We can notice that for all samples the  $\langle P_1 \rangle$  values in the bulk phase is around zero, indicating that, as expected and consistently with the planar alignment, there is no polar alignment of the 5CB molecules with cyano groups pointing toward a preferential direction. A slight increase of the  $\langle P_1 \rangle$  values next to the interfaces with polymer can also be noticed, probably due to some molecules that diffuse in the polymer films.

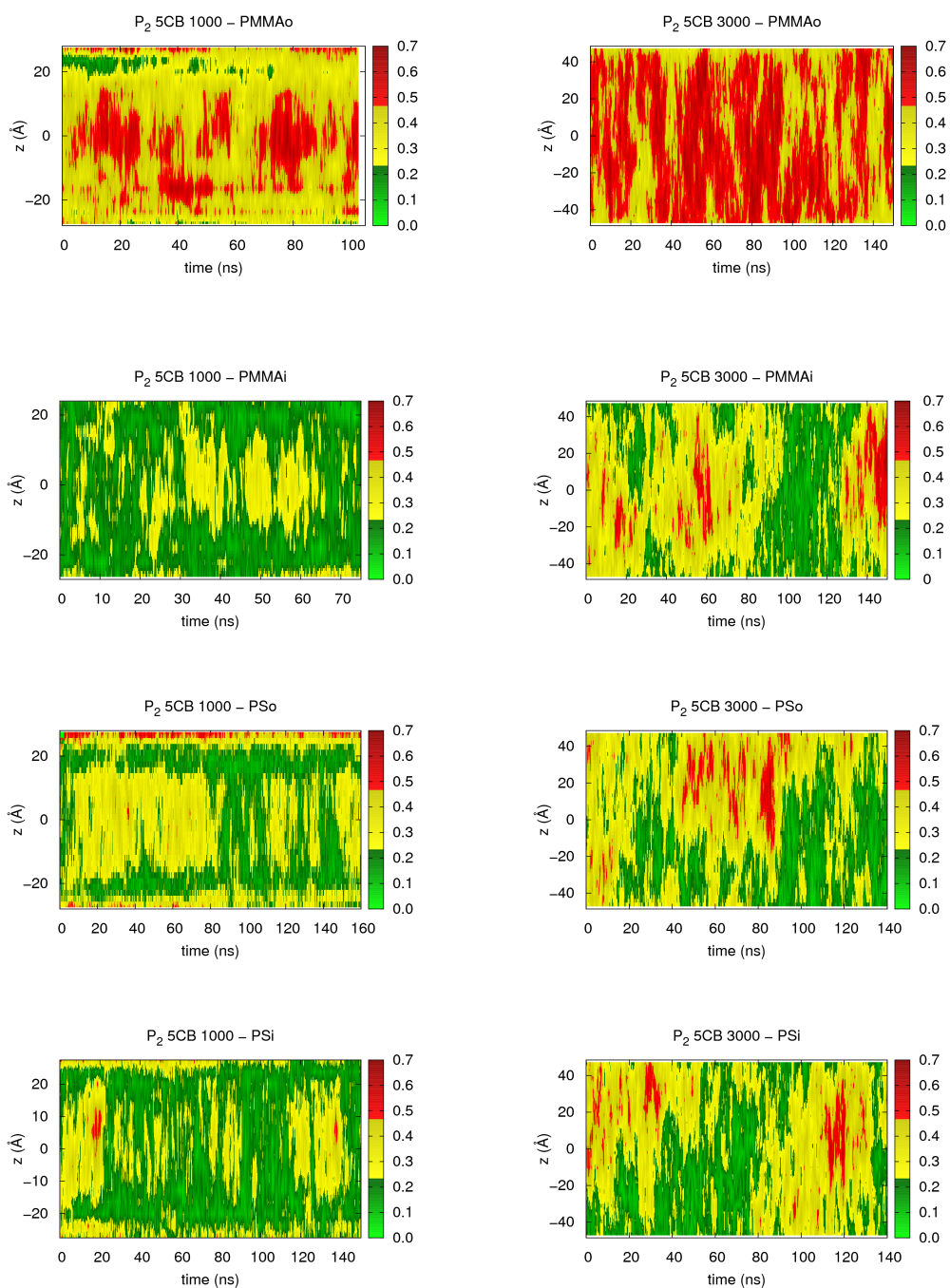


Figure 6.15: Time evolution for the orientational order parameter  $P_2$ , calculated in 0.5 nm wide slabs along the z coordinate of the simulation box, for samples composed by 1000 (left) and 3000 (right) molecules of 5CB.

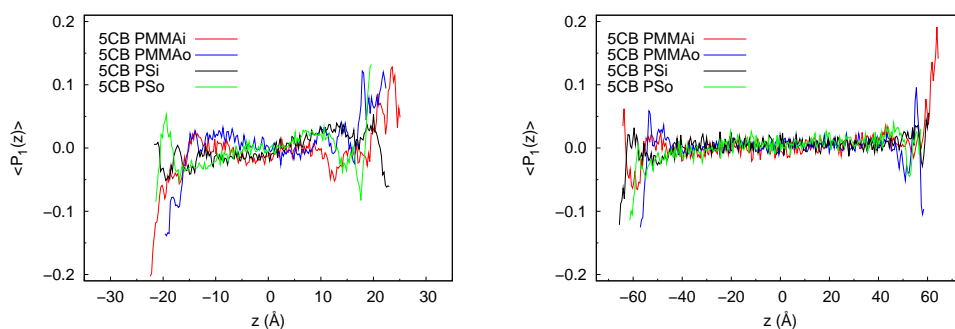


Figure 6.16: 5CB polar order parameter  $\langle P_1 \rangle$  as a function of  $z$  for samples with 1000 (right) and with 3000 (left) molecules of 5CB

#### 6.2.4 Microscopic origin of 5CB surface alignment

It is worth investigating whether exist specific interactions that orient the LC molecules and determine the surface easy axis. For that purpose in Figure 6.19 we show, values of  $\langle P_2 \rangle$  for PS phenyl side groups in the para-direction (see Figure 6.18), as a function of the  $z$  axis of the simulation box. We can notice that, in proximity of the surface, phenyls tend to be more ordered than in the PS bulk phase, and are oriented with the para axis perpendicular to the surface and toward the LC phase. This is in agreement with the experimental results which found the phenyl rings, in rubbed PS, to be aligned in the direction perpendicular to the rubbing one and tilted from the surface normal with a large distribution of angles<sup>[65]</sup>. This also was seen in hybrid atomistic-coarse grained simulations of polystyrene-vacuum interfaces. Phenyl side rings are found to be tilted with respect to the normal the PS surface of  $\sim 30^\circ$ - $40^\circ$  at 303 K in vacuum<sup>[66]</sup>. From values of  $\langle P_2 \rangle$  for PS phenyl side groups in the ortho-direction reported in Figure 6.20, it can be seen that phenyls tend to align with this axis along the  $y$  direction. So the observed alignment of LC phase perpendicularly to the chain stretching direction is probably due the  $\pi$ - $\pi$  interaction of the 5CB aromatic moieties with the phenyl PS side groups lying with their para direction toward the LC phase and the ortho direction pointing nearly per-

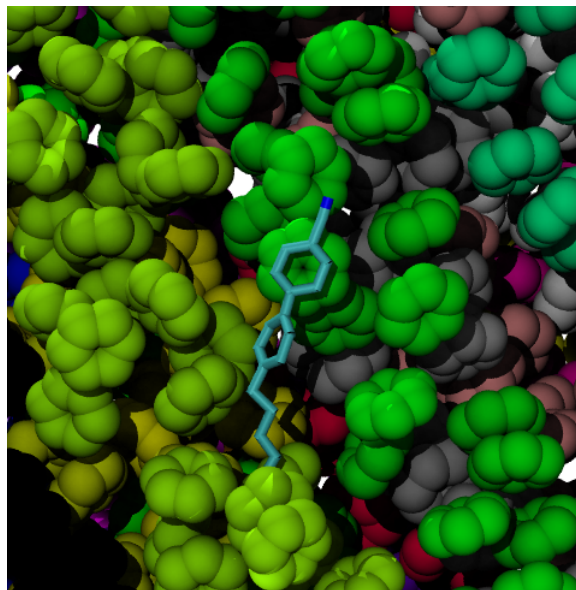


Figure 6.17: Example of  $\pi$  - $\pi$  interaction between the 5CB and PS phenyl moieties.

pendicular to the backbone direction (see Figure 6.17). Instead the origin of microscopic 5CB alignment on PMMAo surface, seems to be due to its interactions with polymer backbones well oriented along the stretching directions as can be seen from Figure 6.21.

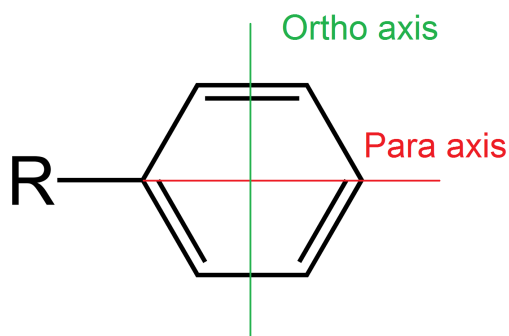


Figure 6.18: Schematic picture of the chosen reference directions for PS phenyl side rings: para axis (red) and ortho axis (green).

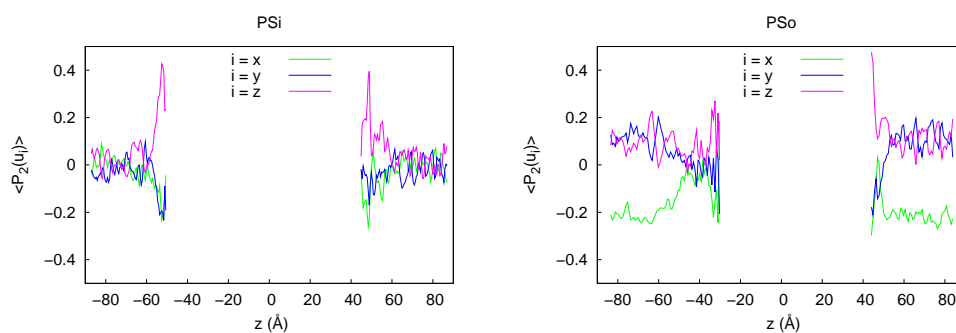


Figure 6.19: Cartesian component of the average orientational order parameter  $\langle P_2 \rangle$  of phenyl side groups, calculated along the para-direction, as a function of z coordinate of the simulation box, for samples composed 3000 (right) molecules of 5CB.

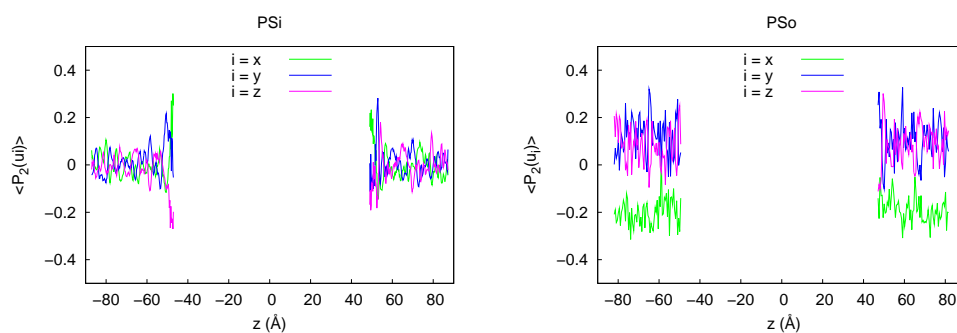


Figure 6.20: Cartesian component of the average orientational order parameter  $\langle P_2 \rangle$  of phenyl side groups, calculated along the direction perpendicular to the para, as a function of z coordinate of the simulation box, for samples composed of 3000 (right) molecules of 5CB.

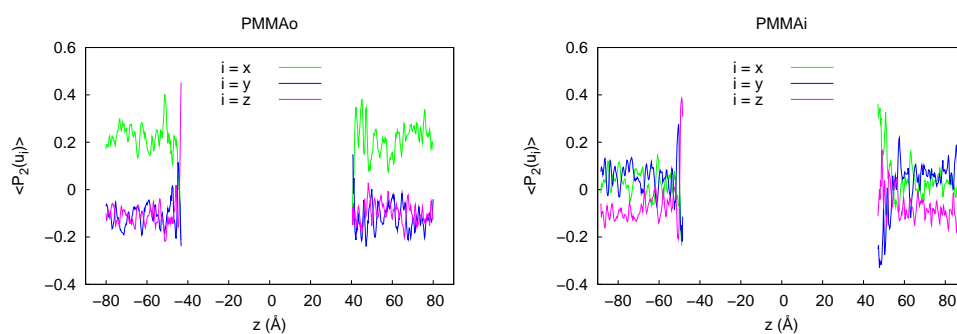


Figure 6.21: Average orientational order parameter  $\langle P_2 \rangle$  of phenyl side groups, calculated along PMMA backbone-direction, as a function of z coordinate of the simulation box, for samples composed 3000 (right) molecules of 5CB.



# Chapter 7

## Conclusions

Polymeric surfaces of PS and PMMA with different degree of molecular order were studied at the interface with the 5CB liquid crystal through atomistic MD simulations. The samples considered were composed of different number of 5CB molecules, respectively 1000 and 3000. Values of the end-to-end vector, gyration radius of polymer chains and surface roughness were calculated to confirm that flat amorphous and ordered polymer substrates were created properly. In ordered samples, chains were planar stretched along one direction, in the same way they are supposed to be in a rubbed polymer substrate. In disordered samples, chain were isotropically oriented in a random coil conformation as in the case of amorphous polymers. As shown from density profiles 5CB molecules tend to diffuse in each sample for  $\sim 1-2$  nm. All samples, independently of polymer chains orientation, present a planar homogeneous 5CB molecular organization at the surface, without a polar order of the cyano 5CB group. All surfaces were observed to induce orientational disorder on the LC phase, that presents only a weak nematic behaviour at the simulation temperature (300 K). The only sample which present a truly nematic behaviour is ordered PMMA with 3000 molecules. Interestingly, as found in experimental studies, PMMA exhibits LC molecules orientation along the stretching direction of chains. On PS surface, 5CB molecules are oriented perpendicularly to the stretching direction, due to the interaction of the respective polymer/LC aromatic moieties. In fact phenyl rings were found to

be tilted with respect to the surface towards the LC phase and aligned perpendicularly to the rubbing direction. In conclusion the presented results show that, probably, in the studied polymers, both chains stretching and polymer functionalization contributes to the orientational order of the liquid crystal phase, and that the surface microgrooves created by rubbing are not necessary to reproduce the experimental results for the alignment of 5CB on PS and PMMA surfaces.

# Bibliography

- [1] Jan P. F. Lagerwall and G. Scalia. A new era for liquid crystal research: Applications of liquid crystals in soft matter nano-, bio- and microtechnology. *Curr. Appl. Phys.*, 12:1387 – 1412, 2012.
- [2] Mauguin C. Sur les cristaux liquides de lehmann. *Bull. Soc. fr. Min.*, 34:71–117, 1911.
- [3] K. L. Mittal and K. W. Lee. *Polymer Surfaces and Interfaces: Characterization, Modification and Application*. VSP, 1997.
- [4] M. B. Hamaneh and P. L. Taylor. Simulated anchoring of a nematic liquid crystal at a polymer surface. *Phys. Rev. E*, 77:021707, Feb 2008.
- [5] A. Pizzirusso, R. Berardi, L. Muccioli, M. Ricci, and C. Zannoni. Predicting surface anchoring: molecular organization across a thin film of 5cb liquid crystal on silicon. *Chem. Sci.*, 3:573–579, 2012.
- [6] O. M. Roscioni, L. Muccioli, R. G. Della Valle, A. Pizzirusso, M. Ricci, and C. Zannoni. Predicting the anchoring of liquid crystals at a solid surface: 5-cyanobiphenyl on cristobalite and glassy silica surfaces of increasing roughness. *Langmuir*, 0:null, 2013.
- [7] T.J. Sluckin, D.A. Dunmur, and H. Stegemeyer. *Crystals That Flow: Classic Papers from the History of Liquid Crystals*. Liquid Crystals Book Series. Taylor & Francis, 2004.

- [8] V. Freedericksz and V. Zolina. Forces causing the orientation of an anisotropic liquid. *Trans. Faraday Soc.*, 29:919–930, 1933.
- [9] H. Zocher. The effect of a magnetic field on the nematic state. *Trans. Faraday Soc.*, 29:945–957, 1933.
- [10] A. S. C. Lawrence. Lyotropic mesomorphism. *Trans. Faraday Soc.*, 29:1008–1015, 1933.
- [11] Liquid crystals and anisotropic melts. a general discussion held by the faraday society. *J. Phys. Chem.*, 38:247–248, 1933.
- [12] D. Demus. *Handbook of Liquid Crystals: Fundamentals*, volume 1 of *Handbook of Liquid Crystals*. Wiley-VCH, 1998.
- [13] M. J. Stephen and J. P. Straley. Physics of liquid crystals. *Rev. Mod. Phys.*, 46:617–704, 1974.
- [14] I. Dierking. *Textures of Liquid Crystals*. Wiley, 2006.
- [15] A. Ferrarini, S. Pieraccini, S. Masiero, and G. P. Spada. Chiral amplification in a cyanobiphenyl nematic liquid crystal doped with helicene-like derivatives. *Beilstein J. Org. Chem.*, 5:50, 2009.
- [16] S. Chandrasekhar, B. K. Sadashiva, and K. A. Suresh. Liquid crystals of disc-like molecules. *Pramana*, 9:471–480, 1977.
- [17] P. Semenza. Can anything catch TFT LCDs? *Nat. Photon.*, 1, 2007.
- [18] I-Hsin Lin, D. S. Miller, P. J. Bertics, C. J. Murphy, J. J. de Pablo, and N. L. Abbott. Endotoxin-induced structural transformations in liquid crystalline droplets. *Science*, 332:1297–1300, 2011.
- [19] M. O'Neill and S. M. Kelly. Ordered materials for organic electronics and photonics. *Adv. Mater.*, 2011.
- [20] M. Ravnik and Slobodan Z. Nematic colloids entangled by topological defects. *Soft Matt.*, 5:269–274, 2009.

- [21] M. Nakata, M. Sato, Y. Matsuo, S. Maeda, and S. Hayashi. Hollow fibers containing various display elements: A novel structure for electronic paper. *J. Soc. Inf. Disp.*, 14:723–727, 2006.
- [22] M. Warner and E.M. Terentjev. *Liquid Crystal Elastomers*. International Series of Monographs on Physics. OUP Oxford, 2007.
- [23] A. Di Nola, D. Roccatano, and H. J. C. Berendsen. Molecular dynamics simulation of the docking of substrates to proteins. *Prot. Struct., Funct., and Bioinf.*, 19:174–182, 1994.
- [24] J.Meller. *Molecular Dynamics*. John Wiley & Sons Ltd, 2001.
- [25] R. Car and M. Parrinello. Unified approach for molecular dynamics and density-functional theory. *Phys. Rev. Lett.*, 55:2471, 1985.
- [26] R. J. Sadus. *Molecular Simulation of Fluids: Theory, Algorithms and Object-Oriented*. Elsevier Science Limited, 2002.
- [27] D. Frenkel and B. Smit. *Understanding Molecular Simulation: From Algorithms to Applications*. Computational science. Elsevier Science, 2001.
- [28] L. Verlet. Computer "experiments" on classical fluids. I. Thermodynamical properties of Lennard-Jones molecules. *Phys. Rev.*, 159:98–103, 1967.
- [29] K. Y. Hyyoshi. Constant-temperature molecular dynamics. *J.Phys.: Condens.Matter*, 2:115–119, 1990.
- [30] S. B. Sinnott Y. Hu. Constant temperature molecular dynamics simulations of energetic particle-solid collisions: comparison of temperature control methods. *J.Comp. Phys.*, 200:252–266, 2004.
- [31] H. J. C. Berendsen, J. P. M. Postma, W. F. van Gunsteren, A. Di Nola, and J. R. Haak. Molecular dynamics with coupling to an external bath. *J. Chem. Phys.*, 81:3684–3690, 1984.

- [32] D. Fincham and D. M. Heyes. Recent advances in molecular dynamics computer simulation. *Adv. Chem. Phys.*, 63:493–575, 1985.
- [33] D. Frenkel and B. Smit. *Understanding Molecular Simulations: From Algorithms to Applications*. Academic Press, San Diego, 1996.
- [34] E. Procacci and M. Marchi. Taming the Ewald sum in molecular dynamics simulations of solvated proteins via a multiple time step algorithm. *J. Phys. Chem*, 104:3003–3012, 1996.
- [35] M. Parrinello and A. Rahman. Polymorphic transitions in single crystals: A new molecular dynamics method. *J. Appl. Phys.*, 52:7182–7190, 1981.
- [36] M. P. Allen and D. J. Tildesley. *Computer Simulation of Liquids*. Oxford University Press, Walton Street, Oxford OX2 6DP, 1989.
- [37] J. Wang, P. Cieplak, and P. A. Kollman. How well does a restrained electrostatic potential (RESP) model perform in calculating conformational energies of organic and biological molecules? *J. Comput. Chem.*, 21:1049, 2000.
- [38] W. L. Jorgensen and N. A. McDonald. Development of an all-atom force field for heterocycles. properties of liquid pyridine and diazenes. *Theochem - J. Mol. Str.*, 424:145–155, 1998.
- [39] W. F. van Gunsteren and H. J. C. Berendsen. *Groningen Molecular Simulation (GROMOS) Library Manual*. Biomos, Groningen, 1987.
- [40] Polygen Corp. Parameter and topology files for charmm, version 22, Copyright 1986, Release 1992.
- [41] A. K. Rappè, C. J. Casewit, K. S. Colwell, W. A. Goddard, and W. M. Skiff. Uff, a full periodic table force field for molecular mechanics and molecular dynamics simulations. *J. Am. Chem. Soc.*, 114:10024–10035, 1992.

- [42] N. L. Allinger, Y. H. Yuh, and J. Lii. Molecular mechanics. the mm3 force field for hydrocarbons. 1. *J. Am. Chem. Soc.*, 111:8551, 1989.
- [43] S. K. Nath and R. Khare. New force field parameters for branched hydrocarbons. *J. Chem. Phys.*, 115:10837, 2001.
- [44] H. Sun. Compass: an ab initio force field optimized for condensed-phase applications overview with details on alkane and benzene compounds. *J. Phys. Chem. B.*, 102:7338–7364, 1998.
- [45] A. C. T. van Duin, S. Dasgupta, F. Lorant, and W. A. Goddard III. Reaxff: A reactive force field for hydrocarbons. *J. Phys. Chem. A*, 105:9396–9409, 2001.
- [46] A. D. Mackerell. Empirical force fields for biological macromolecules: Overview and issues. *J. Comput. Chem.*, 25:1584–1604, 2004.
- [47] K. S. Pitzer and W. D. Gwinn. Energy levels and thermodynamic functions for molecules with internal rotation i. rigid frame with attached tops. *J. Chem. Phys.*, 10:428–440, 1942.
- [48] P. Cieplak, W. D. Cornell, C. Bayly, and P. A. Kollmann. Application of the multimolecule and multiconformational RESP methodology to biopolymers: Charge derivation for DNA, RNA, and proteins. *J. Comput. Chem.*, 16:1357–1377, 1995.
- [49] H. S. Antila and E. Salonen. *Polarizable Force Fields*, volume 924 of *Methods in Molecular Biology*. Humana Press, 2013.
- [50] J. Ally, E. Vittorias, A. Amirfazli, M. Kappl, E. Bonaccorso, C. E. McNamee, and H.-J. Butt. Interaction of a microsphere with a solid-supported liquid film. *Langmuir*, 26:11797–11803, 2010.
- [51] A. N. Zelikin. Drug releasing polymer thin films: New era of surface-mediated drug delivery. *ACS Nano*, 4:2494–2509, 2010.

- [52] J. Zhang and Y. Han. Active and responsive polymer surfaces. *Chem. Soc. Rev.*, 39:676–693, 2010.
- [53] J. Wang, Z. Paszti, M. A. Even, and Z. Chen. Measuring polymer surface ordering differences in air and water by sum frequency generation vibrational spectroscopy. *J. Am. Chem. Soc.*, 124:7016–7023, 2002.
- [54] M. Schadt and W. Helfrich. Voltage-dependent optical activity of a twisted nematic liquid crystal. *Appl. Phys. Lett.*, 18:127–128, 1971.
- [55] M. Oh-e and K. Kondo. Electro-optical characteristics and switching behavior of the in-plane switching mode. *Appl. Phys. Lett.*, 67:3895–3897, 1995.
- [56] A. Takeda, S. Kataoka, T. Sasaki, H. Chida, H. Tsuda, K. Ohmuro, T. Sasabayashi, Y. Koike, and K. Okamoto. A super-high image quality multi-domain vertical alignment lcd by new rubbing-less technology. *SID Symp. Dig. Tech. Pap.*, 29:1077–1080, 1998.
- [57] T. Miyashita, P. J. Vetter, Y. Yamaguchi, and T. Uchida. Wide-viewing-angle display mode for active-matrix lcds using a bend-alignment liquid-crystal cell. *J. Soc. Inf. Disp.*, 3:29–34, 1995.
- [58] G. H. Suk, K. Yong-Gi, R. Yecheol, A. Byungcheol, and R. Moonhor. Liquid crystal alignment in advanced flat-panel liquid crystal displays. *Curr. Op. Chem. Eng.*, 2:71 – 78, 2013.
- [59] S. Ishihara. How far has the molecular alignment of liquid crystals been elucidated ? *J. Disp. Techn.*, 1:30–40, 2005.
- [60] J. M. Geary, J. W. Goodby, A. R. Kmetz, and J. S. Patel. The mechanism of polymer alignment of liquid-crystal materials. *J. of Appl. Phys.*, 62:4100–4108, 1987.

- [61] S. Ishihara, H. Wakemoto, K. Nakazima, and Y. Matsuo. The effect of rubbed polymer films on the liquid crystal alignment. *Liq. Cryst.*, 4:669–675, 1989.
- [62] S. G. Hahm, T. J. Lee, T. Chang, J. C. Jung, W.-C. Zin, and M. Ree. Unusual alignment of liquid crystals on rubbed films of polyimides with fluorenyl side groups. *Macromolecules*, 39:5385–5392, 2006.
- [63] S. W. Lee, J. Yoon, H. C. Kim, B. Lee, T. Chang, and M. Ree. Effect of molecular weight on the surface morphology, molecular reorientation, and liquid crystal alignment properties of rubbed polystyrene films. *Macromolecules*, 36:9905–9916, 2003.
- [64] S. W. Lee, B. Chae, H. C. Kim, B. Lee, W. Choi, S. B. Kim, T. Chang, and M. Ree. New clues to the factors governing the perpendicular alignment of liquid crystals on rubbed polystyrene film surfaces. *Langm.*, 19:8735–8743, 2003.
- [65] Oh e M., Seok-Cheol H., and Y. R. Shen. Orientations of phenyl side-groups and liquid crystal molecules on a rubbed polystyrene surface. *Appl. Phys. Lett.*, 80:784–786, 2002.
- [66] V. Marcon, D. Fritz, and N. F. A. van der Vegt. Hierarchical modelling of polystyrene surfaces. *Soft Matter*, 8:5585–5594, 2012.
- [67] A. Sugimura and O.-Y. Zhong-can. Mechanism of nematic molecular alignment based on friction charges and surface topology by rubbing. *Liq. Cryst.*, 14:319–326, 1993.
- [68] G. Barbero, L.R. Evangelista, and N.V Madhusudana. Effect of surface electric field on the anchoring of nematic liquid crystals. *Europ. Phys. J. B - Cond. Matt. Comp. Syst.*, 1:327–331, 1998.
- [69] K. E. Gubbins and J. D. Moore. Molecular modeling of matter: Impact and prospects in engineering. *Ind. Eng. Chem. Res.*, 49:3026–3046, 2010.

- [70] I. H. Bechtold, M. P. De Santo, J. J. Bonvent, E. A. Oliveira, R. Barberi, and T. H. Rasing. Rubbing-induced charge domains observed by electrostatic force microscopy: effect on liquid crystal alignment. *Liq. Cryst.*, 30:591–598, 2003.
- [71] W. D. Cornell, P. Cieplak, C. I. Bayly, I. R. Gould, K. M. Merz, D. M. Ferguson, D. C. Spellmeyer, T. Fox, J. W. Caldwell, and P. A. Kollman. A second generation force field for the simulation of proteins, nucleic acids, and organic molecules. *J. Am. Chem. Soc.*, 117:5179–5197, 1995.
- [72] N. G. Martinelli, M. Savini, L. Muccioli, Y. Olivier, F. Castet, C. Zannoni, D. Beljonne, and J. Cornil. Modeling polymer dielectric/pentacene interfaces: On the role of electrostatic energy disorder on charge carrier mobility. *Adv.Func. Mat.*, 19:3254–3261, 2009.
- [73] J.E. Mark. *Physical Properties of Polymers Handbook*. Springer London, Limited, 2007.
- [74] P. G. Santangelo and C. M. Roland. Molecular weight dependence of fragility in polystyrene. *Macromolecules*, 31:4581–4585, 1998.
- [75] U. Koichi, M. Nobuo, and H. Koichi. Glass transition temperature and melting temperature of uniform isotactic and syndiotactic poly(methyl methacrylate)s from 13mer to 50mer. *Polymer*, 36:1415 – 1419, 1995.
- [76] E. F. Scott, Z. Yuhong, W. P. Richard, and R. B. Bernard. Constant pressure molecular dynamics simulation: The langevin piston method. *J.Chem. Phys.*, 103:4613–4621, 1995.
- [77] G. Tiberio, L. Muccioli, R. Berardi, and C. Zannoni. Realistic transition temperatures and physical properties for n-cyanobiphenyls via molecular dynamics simulations. *ChemPhysChem*, 10:125–136, 2009.

- [78] J. C. Phillips, R. Braun, W. Wang, J. Gumbart, E. Tajkhorshid, E. Villa, C. Chipot, R. D. Skeel, L. Kale, and K. Schulten. Scalable molecular dynamics with NAMD. *J. Comput. Chem.*, 26:1781–1802, 2005.
- [79] U. Essmann, L. Perera, M. L. Berkowitz, T. Darden, H. Lee, and L. G. Pedersen. A smooth particle mesh Ewald method. *The J. of Chem. Phys.*, 103:8577–8593, nov 1995.
- [80] M. Sandmann A. Wuerflinger. *Physical Properties of Liquid Crystals*, volume 1 Nematics, (eds. D. A. Dunmur, A. Fukuda, G. R. Luckhurst). IEE, London, 2001.
- [81] E. Bonaccorso and K. Graf. Nanostructuring effect of plasma and solvent treatment on polystyrene. *Langmuir*, 20:11183 – 11190, 2004.
- [82] L. Lin, Y.T. Cheng, and J.C. Chiu. Comparative study of hot embossed micro structures fabricated by laboratory and commercial environments. *Mycrosist. Techn.*, 4:113–116, 1998.
- [83] H. Hori, O. Urakawa, and K. Adachi. Dielectric relaxation in phase-segregated mixtures of polystyrene and liquid crystal 5cb. *Macromolecules*, 37:1583–1590, 2004.
- [84] T.Yoshizaki T.Konishi, Y.Einaga T.Saito, and H.Yamakawa. Mean-square radius of gyration of oligo- and polystyrenes in dilute solutions. *Macromolecules*, 23:290–297, 1990.
- [85] Y.Einaga F.Abe, K.Horita and H.Yamakawa. Excluded-volume effects on the mean-square radius of gyration and intrinsic viscosity of oligo- and poly(methylmethacrylate)s. *Macromolecules*, 27:725–732, 1994.
- [86] M. F. Palermo, A. Pizzirusso, L. Muccioli, and C. Zannoni. An atomistic description of the nematic and smectic phases of 4-n-octyl-4'-cyanobiphenyl (8CB). *J. Chem. Phys.*, 138:204901, 2013.

- [87] Michael I. Kinsinger, Maren E. Buck, Maria-Victoria Meli, Nicholas L. Abbott, and David M. Lynn. Langmuir films of flexible polymers transferred to aqueous/liquid crystal interfaces induce uniform azimuthal alignment of the liquid crystal. *J. Coll. Int. Sci.*, 341:124 – 135, 2010.
- [88] S. Ishihara, H. Wakemoto, K. Nakazima, and Y. Matsuo. The effect of rubbed polymer films on the liquid crystal alignment. *Liq. Cryst.*, 4:669–675, 1989.